2020

Initial Transformation of Photo-Viable Free Amino Acids in the Presence of Surrogate and Standard Dissolved Organic Matter Under Sunlit Irradiation

Ryan J. Kibler

INITIAL TRANSFORMATION OF PHOTO-VIABLE FREE AMINO ACIDS IN THE PRESENCE OF SURROGATE AND STANDARD DISSOLVED ORGANIC MATTER UNDER SUNLIT IRRADIATION

By

Ryan J. Kibler

A THESIS

Submitted in partial fulfillment of the requirements for the degree of

MASTER OF SCIENCE

In Environmental Engineering

MICHIGAN TECHNOLOGICAL UNIVERSITY

2020

This thesis has been approved in partial fulfillment of the requirements for the Degree of MASTER OF SCIENCE in Environmental Engineering.

Department of Civil and Environmental Engineering

Thesis Advisor:	*Dr. Daisuke Minakata*
Committee Member:	*Dr. Paul Doskey*
Committee Member:	*Dr. Sarah Green*
Department Chair:	*Dr. Audra Morse*

Table of Contents

List of figures

List of tables

Acknowledgements

I would like to thank my advisor, Dr. Daisuke Minakata, who has continually given amazing support and mentorship during my graduate studies. Words cannot express the gratitude that I owe to him. His dedication and availability to his students is unmatched by any faculty. He believed in me, even when I had my own doubts, which I am so grateful for. Thank you for instilling a love for research and motivating me to never give up, no matter how difficult the obstacles are.

I also would like to acknowledge the support of my committee members, Dr. Sarah Green and Dr. Paul Doskey, who have been so flexible as I finished my thesis. All of the faculty at Michigan Tech, particularly those in Civil and Environmental Engineering, will always hold such a special place in my heart. Thank you for making Michigan Tech such an amazing place to call my alma mater for both my BS and MS.

None of my graduate research studies could have been completed without the support from the National Science Foundation CHE-1808052, the Michigan Space Grant Consortium, the Great Lakes Research Center, and the Civil and Environmental Engineering.

Finally, I would like to thank my family and friends for supporting me throughout my MS degree. Additionally, thank you for the lifelong friendship from JP Harron who has been a huge support throughout my graduate career. In particular, thank you to my parents and wife, Lisa, for your continued love and support throughout my undergraduate and graduate studies.

With love,

Ryan Kibler

Abstract

With more than half of the nation's drinking water affected by wastewater discharge from upstream and more indirect and direct reuse of treated wastewater, human health and ecotoxicological impacts resulting from effluent organic material (EfOM) will increase. Dissolved free amino acids (DFAAs), nitrogen components of EfOM, are essential nitrogen sources for microorganisms and play important roles in global N-cycling in natural aquatic environments. Several DFAAs including histidine, methionine, and tyrosine in sunlit surface waters are susceptible to direct and indirect photochemical transformation with reactive oxygen species. In this study, we investigated the reaction kinetics and initial reaction mechanisms involved in the fate of DFAAs through temperature-dependent bench-top photolysis experiments. Three prevalent surrogate DOM compounds were chosen (1,4-naphthoquinone, umbelliferone, 2-naphthaldehyde) which have been shown to be critical photosensitizers in the natural environment leading to the production of photochemically-produced reactive intermediates (PPRI) such as singlet oxygen ($^1O_2$), excited triplet state CDOM ($^3CDOM^*$), and hydroxyl radicals ($HO^\bullet$). All chosen surrogate DOM compounds and amino acids are structurally unique generating distinct degradation pathways of amino acids at three different temperatures (10 °C, 20 °C, 30 °C).

1 Introduction

Dissolved amino acids (both free and combined amino acids), which comprise a significant fraction of dissolved organic nitrogen (DON) in effluent organic matter are major sources of nitrogen and carbon in freshwater systems. Combined amino acids account for approximately 10-20% of wastewater DON.[1] In the aquatic environment, DON is a limiting nutrient making it a valuable source for the environmental microbiome.[2] Although the amino acids comprise a few percent of dissolved free amino acids[3], dissolved free amino acids are considered 'rare' for the abundance and 'expensive' for the higher free energies of formation required[3]. Consequently, understanding the fate of free amino acids in the natural aquatic environment is a critical component of global nitrogen cycling[4] as well as global sulfur cycling[5].

Abiotic photochemical oxidation is a major transformation pathway of free amino acids in sunlit waters. Of the 20 proteinogenic free amino acids, only five (i.e., tryptophan, tyrosine, histidine, methionine, and cysteine) are susceptible to photochemical degradation.[6] Photochemical oxidation occurs through direct photolysis of amino acids and indirect oxidation by dissolved photochemically produced reactive intermediates (PPRI), which are transient, short-lived chemical species produced from excitation of chromophores and interaction with dissolved oxygen. Direct photolysis depends on the absorbance of sunlight by the AAs relative to the emission of sunlight over the same wavelengths.[6] Indirect oxidation occurs by PPRI such as excited triplet state (^{3}CDOM*) of DOM generated by photolysis of chromophoric DOM (CDOM)[6,7,8,9] , singlet oxygen ($^1O_2$)[10], hydroxyl radicals ($HO^\bullet$)[11], and hydrogen peroxide (H_2O_2)[12,13].

Photolysis-induced excitation of a complex mixture of CDOM that has numerous chromophoric functional groups and short-lived reactive PPRI makes it challenging to understand the photochemical reaction pathways and kinetics in the heterogeneous system.

Although the initial transformations of various photo-viable free amino acids have been investigated under different solution pH conditions, the fate of free amino acids under sunlight irradiation in natural aquatic environment has not been elucidated yet. For example, tyrosine and tryptophan found to be susceptible to direct photolysis due to their spectral absorbance overlap in the UV-vis range.[3, 6, 14] Histidine was predominantly degraded by $^1O_2$, while the predominant pathway of methionine, tyrosine, and tryptophan was via $^3CDOM^*$ interaction.[3, 6, 14-16] Cysteine's pH dependence degradation was found to attribute lower quenching rates of $^3CDOM^*$ by molecular oxygen[17]. Faster reaction rates of both histidine and histamine at higher pH[15] were observed. Tryptophan's degradation via direct photolysis and indirect photodegradation via its interaction with primarily $^3CDOM^*$ was confirmed[3]. These previous studies have been limited to well-studied sensitizers such as reference DOM isolates, lumichrome, perinaphthenone, and riboflavin. Thus, knowledge gaps remain in the role of chromophoric functional groups of CDOM and mechanistic understandings of elementary reaction photochemical pathways under different solution temperatures.

The solution temperature is one of the most important factors affecting the fate of free amino acid photochemical degradation (Figure 1). Initially, the chromophoric DOM is known to absorb photons and excite electrons to form a single excited state of CDOM

(i.e., ^{1}CDOM*). This ^{1}CDOM* undergoes intersystem crossing (ISC) to form a tripled excited state (i.e., ^{3}CDOM*). The ^{3}CDOM* is known to undergo two major pathways: (1) relaxation to a ground state CDOM and (2) reaction with ground state dissolved oxygen in water. The first order rate constants of ^{3}CDOM* relaxation ranges from 6×10^{4} to 1.2×10^{5} s^{-1} [18] and the solution temperature affects the dominant non-radiative relaxation resulting from intramolecular mechanism.[19, 20] The reaction of ^{3}CDOM* with $^{3}O_2$ to produce a singlet oxygen (i.e., $^{1}O_2$) is temperature-dependent (1-6 $\times$ 10^{9} $M^{-1}s^{-1}$ for small molecular sensitizers) via single electron transfer that is driven by the energy difference between ^{3}CDOM* (i.e., 50-60 kcal/mol)[3, 6, 21-23] and $^{3}O_2$ (i.e., 23 kcal/mol)[16, 24]. The amount of dissolved oxygen also affects this second-order reaction. While the $^{1}O_2$ reacts with dissolved organic compounds, $^{1}O_2$ dominantly undergoes non-radiative relaxation whose temperature-dependent first order reaction rate constants are known to be 2.6-2.8 $\times$ 10^{5} s^{-1} [18, 25]. Given that the major known initial photochemical pathways described above are affected by the solution temperature, free amino acids' degradation is hypothesized to be significantly affected by the solution temperature. For example, if the Arrhenius activation parameters were assumed to have an activation energy of 50 kJ/mol and follow the pseudo-first order decay, an increase in the solution temperature by 5 °C (from 20 °C to 25 °C) would affect the rate constant difference by a factor of 140%.

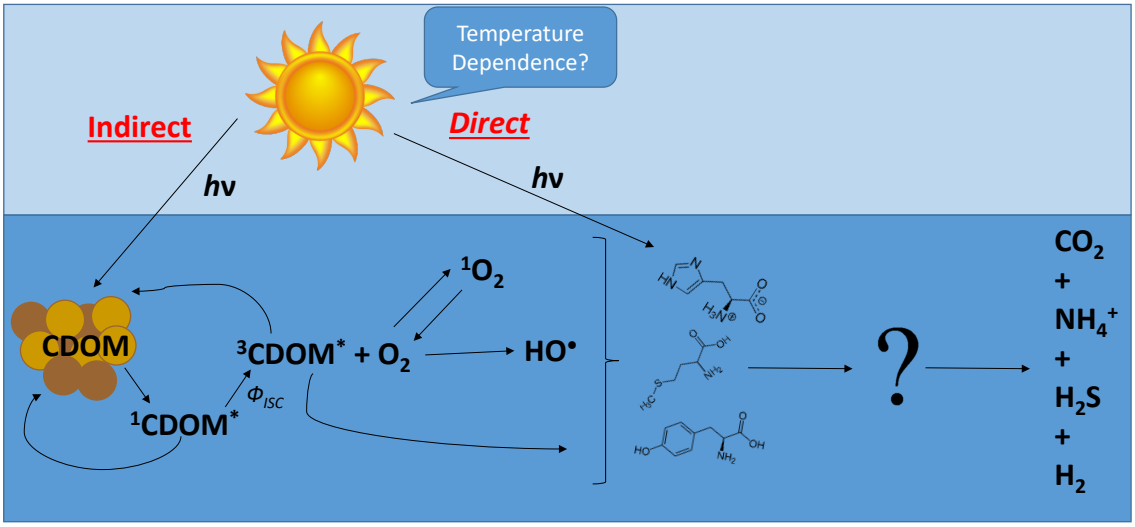

Figure 1: Direct and Indirect Photochemical Reactions of Free Amino Acids

In this study, we investigate the initial reactivities of three photo-viable amino acids (i.e., histidine, tyrosine, and methionine) in the presence of three surrogate CDOM (i.e., 1,4-naphthoquinone, 2-naphthaldehyde, and umbelliferone) under a laboratory-scale visible light irradiation at pH 7 with 3 different solution temperatures. At the given pH, all the amino acids are zwitterion (i.e., NH_3^+ and COO^-). Three amino acids have their unique functional groups: histidine with a five-membered ring imidazole functional group; methionine with an aliphatic compound that has sulfur functional group; and tyrosine with a benzene ring. Three surrogate CDOM share common DOM structures to a complex mixture of DOM: 1,4-naphthoquinone with carbonyl functional group and quinone structure; 2-naphthaldehyde with aldehyde functional group and naphthalene; and umbelliferone with carbonyl in the six-membered ring. We use both density functional theory quantum mechanical calculations and bench-scale laboratory experiments to provide mechanistic insight into the initial reaction mechanisms. Given

the diverse structures of each surrogate DOM, it is anticipated that each will propagate varying degrees of photochemically produced reactive intermediates (PPRI), thus leading to unique degradation pathways of each amino acid.

2 Experimental Methods and Results

2.1 Chemicals

L-Histidine (≥99.5%), L-Tyrosine (≥99.0%), L-Methionine (≥99.5%), 1,4-naphthoquinone (97%), 2-naphthaldehyde (98%), umbelliferone (99%), borax anhydrous (≥99.0%), sodium phosphate dibasic (≥99.0%), sodium phosphate monobasic (>99.0%), sodium azide (>99.8%), sodium hydroxide (≥ 98%), hydrochloric acid (37%), phosphoric acid (≥85%), acetonitrile (UHPLC grade, ≥99.92), methanol (UHPLC grade, ≥99.92%), 2,4,6-trimethylphenol (97%), 4-chlorobenzoic acid (99%), furfuryl alcohol (98%), 4-nitroanisole (97%), pyridine anhydrous (99.8%) were obtained from Sigma Aldrich. O-phthaldehyde and 3-mercaptopropionic acid in 0.4 M borate buffer and 0.4 N borate buffer (pH 10.2) from Agilent Technologies, Inc.

2.1.1 Free Amino Acids

Of the twenty-one total amino acids, five are susceptible to direct and/or indirect photodegradation – tryptophan, histidine, cysteine, methionine, and tyrosine. In recent publications, tryptophan and cysteine have been of particular interest. The other susceptible amino acids were selected for this study due to their unknown degradation pathways as well as their unique structural characteristics. The selected free amino acids for this study are displayed in Figure 2. This subset of amino acids are structurally diverse and react in different mechanisms under photolysis conditions.

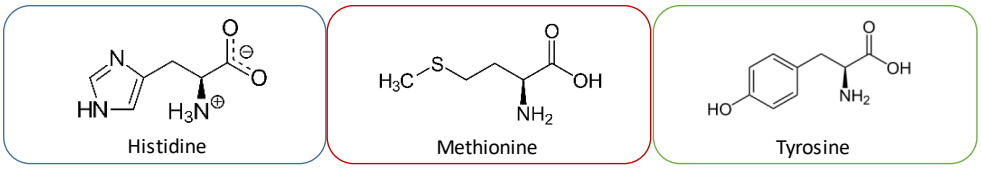

Figure 2. Selected Amino Acids

Tyrosine undergoes both direct photolysis and indirect photolysis via PPRI during photochemical reactions; additionally, tyrosine has an aromatic ring structure with a hydroxyl functional group. Conversely, histidine and methionine only undergo indirect photolysis via reactions with PPRI. Looking specifically, these two amino acids have rather interesting structures. Histidine has a nitrogen heavy structure with an imidazole functional group, whereas methionine has a sulfhydryl functional group. Each of these amino acids will undergo their own unique phototransformation with the diverse structures present.

2.1.2 Surrogate Dissolved Organic Matter

Most studies investigating the fate of organic compounds resulting from photochemical transformation use dissolved organic matter isolates obtained from the International Humic Substances Society (IHSS) such as Suwannee River, Pony Lake, or Nordic Reservoir. These DOM isolates are a complex mixture of hundreds of organic compounds such as aldehydes, ketones, coumarins, and quinones with varying compositions. Rather than relying purely on DOM isolates, this study chose several specific compounds which are known to be prevalent in DOM and are efficient photosensitizers for PPRI. Figure 3 displays the selected surrogate DOM for this study.

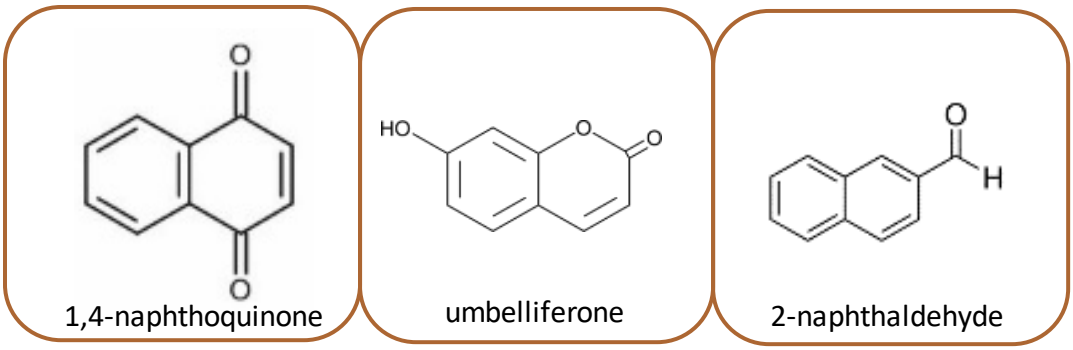

Figure 3. Selected Surrogate Dissolved Organic Matter

To probe the kinetics and feasibility of oxidation/reduction of FAAs by $^{3}CDOM^{*}$ photosensitizers, one must examine the energy level and reduction potential of the surrogate DOM's triplet states. The triplet energies of 1,4-naphthoquinone, umbelliferone, and 2-naphthaldehyde are 241 kJ mol^{-1}, 255 kJ mol^{-1}, and 249 kJ mol^{-1}, respectively[26]. These triplet energies overlap with the average value of 250 kJ mol^{-1} of many surrogate DOM and standard DOM isolates. In their triplet states, 1,4-naphthoquinone, umbelliferone, and 2-naphthaldehyde, their one electron reduction potential are 2.38 V, 1.42 V, and 1.48 V[26]. These one electron reduction potentials are similar to the range of many surrogate $^{3}CDOM^{*}$ [1].

2.2 Photolysis Experiment Design

2.2.1 Experimental Apparatus

All photolysis experiments were carried out using an ATLAS SunTest XLS+ (II) equipped with a 1700 Xe arc lamp which emits photons in the wavelength range of 290 – 800 nm as displayed in Figure 4 below.

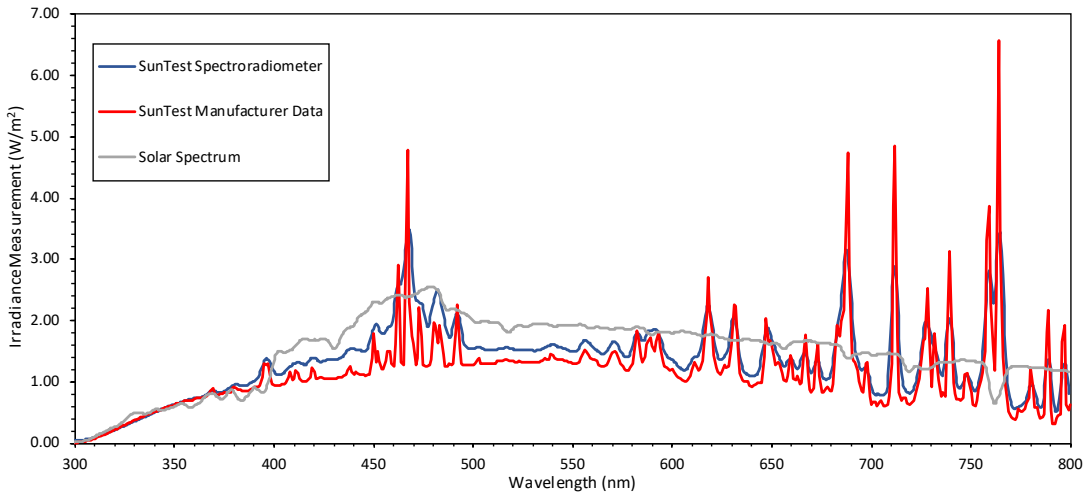

Figure 4. SunTest and Solar Spectrum

The red line portrays the manufacturer reported irradiance spectrum between 300 to 800 nm at a total irradiance of 500 W/m^2. As a validation of our SunTest XLS+ (II), we used our lab's spectroradiometer (StellarNet, Inc. Black Comet) to measure the irradiance values over 300 to 800 nm which is plotted in blue. Finally, it is critical to compare the solar irradiance spectrum to the simulated light of the SunTest. The grey line represents the solar spectrum taken from our rooftop experimental platform at 47.12°N, 88.55° W on July 22nd, 2019 at 2 PM. From this figure, it is evident that the SunTest XLS+ (II) mimics actual sunlight extremely well from 300 to 800 nm, particularly, from 300 to 400 nm. Additionally, the light intensity of the SunTest and solar light was characterized through PNA-pyridine actinometry.

2.2.2 Temperature Controlled System

Upon preliminary investigation using the SunTest XLS+ (II) and custom quartz photoreactors, it was apparent that the experimental solution temperature was quickly

increasing over the duration of the photolysis experiment, nearly 6 °C over the initial 15 minutes (0.4 °C/min). This discovery clearly needed to be addressed by fabricating a water bath which would sit inside of the SunTest's chamber. To address this unique issue, a water bath was constructed to house the quartz photoreactors during photolysis experiments as displayed in Figure 5.

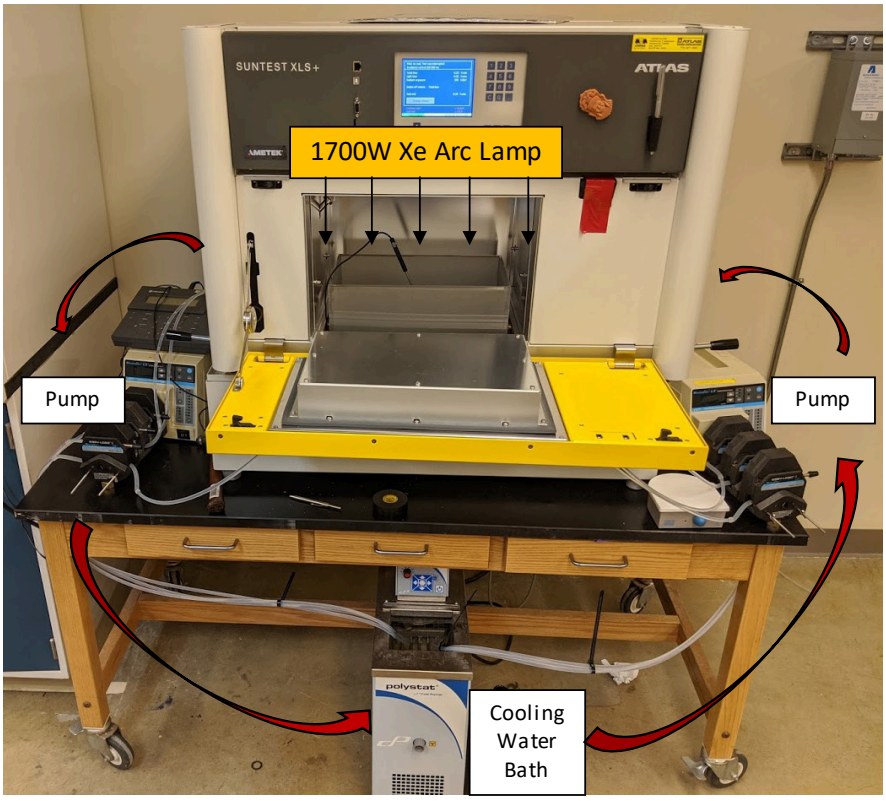

Figure 5. Schematic of Custom Water Bath

The red arrows in Figure 4 display the flow direction of water through the water bath system. Two peristaltic pumps are used to circulate the cooling water from a Cole Parmer Polystat Cooling/Heating Circulating Baths. Each peristaltic pump has three channels which creates a completely mixed flow reactor within the SunTest Chamber.

A custom built water basin was constructed from ¼" acrylic glass lined with an adhesive, stainless steel contact paper as shown in the left panel of Figure 6. The right panel of Figure 6 displays a more deconstructed view of the water basin layout. Three inlet elbows introduce cooling water on the right side of the basin, while, simultaneously, three outlet elbows on the left side of the basin withdraw water to minimize the length of time the cooling water is exposed to the 1700W Xe arc lamp. Custom quartz photoreactors containing the experimental solutions are placed in the water basin. Each photoreactor is placed on four O-rings which are fixed to the bottom of the water basin. This allows for the maximum available surface area for heat transfer from the cooling water to the photoreactors.

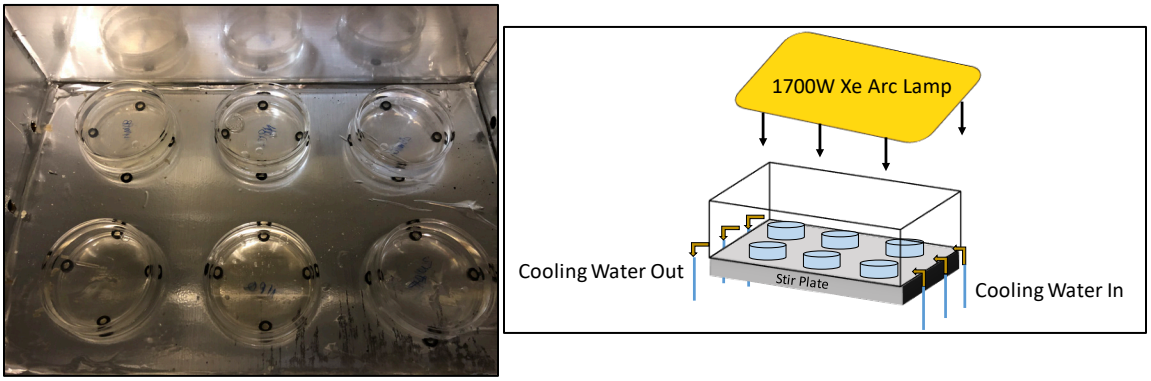

Figure 6. Temperature Controlled Water Basin Design

The peristaltic pumps were operated in a steady-state fashion so that the cooling water depth in the water basin was constant - slightly lower than the height of the quartz photoreactors. Additionally, positioned below the water basin is a six-position magnetic multi-stirrer plate to ensure that all photoreactors are completely mixed.

2.2.3 Experimental Preparation and Procedures

2.2.3.1 Experimental Solutions

2.2.3.1.1 Surrogate DOM and DOM Isolate Experimental Solutions

Experimental solutions used in the photolysis experiments were prepared in bulk. All solutions contained a 1 mM phosphate buffer at a neutral pH of 7. The solutions contained 5 mg C/L of 2-naphthaldehyde, 1,4-naphthoquinone, or umbelliferone. These solutions were allowed to stir continuously for 48 hours to achieve full dissolution of the surrogate DOM prior to use. Additionally, a 5 mg C/L solution was prepared containing Suwannee River humic acid (Standard II) purchased from the International Humic Substances Society (IHSS). All solutions were stored in a temperature controlled room at 4°C in the dark while continuously being stirred for a maximum of 3 weeks.

2.2.3.1.2 Free Amino Acid Stock Solutions

The free amino acid stock solutions containing histidine, tyrosine, or methionine were prepared in 500 mL volumetric flasks at a concentration of 1 mM. These stock solutions were then stored in a temperature controlled room at 4°C in the dark while continuously being stirred for a maximum of 3 weeks.

2.2.3.1.3 Probe Compound Stock Solutions

Furfuryl alcohol, singlet oxygen probe compound, was prepared at a concentration of 1 mM and stored at 4°C. 2,4,6-trimethylphenol, excited triplet state CDOM probe

compound, was prepared at a concentration of 1 mM and continuously stirred at room temperature. Parachlorobenzoic acid, hydroxyl radical probe compound, was prepared at a concentration of 1 mM and continuously stirred at room temperature.

2.2.3.1.4 Experimental Solution Preparation

One day prior to a scheduled experiment, the experimental working solutions were prepared. A 100 mL volumetric flask was filled with the surrogate DOM stock solution followed by the addition of a single target free amino acid (histidine, tyrosine, methionine) or the addition of a single probe compound (furfuryl alcohol, 2,4,6-trimethylphenol, parachlorobenzoic acid). The initial concentration of all free amino acids in solution was 30 μM. The initial concentration of furfuryl alcohol, 2,4,6-trimethlyphenol, and parachlorobenzoic acid was 40 μM, 30 μM, and 10 μM, respectively.

Once the surrogate DOM or DOM isolate solution contained a target free amino acid or probe compound, all solutions were filtered through 0.2 μm nylon membrane filters. Upon filtration, the solutions were transferred to brown borosilicate bottles and stored in a Cole Parmer StableTemp water bath at the specified temperature (10 °C, 20 °C, or 30 °C) for the following day's experiments. This water bath was stored in the temperature controlled room in the dark.

2.2.4 Photolysis Experimental Procedures

On the day of the experiments, approximately 50 mL of the experimental solution was transferred into a custom quartz photoreactors shown in Figure 7. Each photoreactor has a diameter of 6.5 cm and a depth of 2.5 cm with a wall thickness of 2 mm.

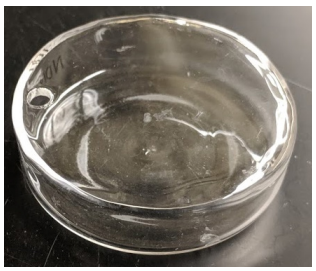

Figure 7. Custom quartz photoreactor

Once transferred, the quartz photoreactors were placed back into the water bath to allow the temperature to re-equilibrate to the specified experimental temperature. After equilibration, the photoreactors were moved into the temperature controlled water bath situated inside of the SunTest XLS + (II) as previously shown in Figure 6 and Figure 6.

The SunTest XLS+ (II) irradiance intensity was set to 500 W/m^2 in the range of 300 – 800 nm. A daylight glass filter manufactured by Atlas was employed to block any irradiance below 290 nm. All photolysis experiments with surrogate DOM were conducted for two hours. With SRHA experimental solutions, the photolysis time was increased to eight hours to achieve sufficient degradation of the target compounds. During the photolysis exposure, 500 µL aliquots were removed at predetermined time intervals, transferred to autosampler vials, then capped and stored in the dark at 4°C. All samples were analyzed on a ThermoFisher Dionex UltiMate 3000 Ultra High

Performance Liquid Chromatography (UHPLC) system. Samples were stored for a maximum of 48 hours before analysis was completed.

2.2.5 UHPLC Methods & Measurements

2.2.5.1 Free Amino Acids

The free amino acids (histidine, tyrosine, methionine) were measured using an online derivatization method utilizing *o*-phthaldiadehyde/3-mercaptopropionic acid (OPA/3-MPA). This method utilizes three derivatization reagents: OPA/3-MPA reagent, borate buffer (pH 10.2), and an injection diluent (100 mL of Mobile Phase A + 0.4 mL phosphoric acid). The online derivatization steps are detailed in Table 1. The mobile phase is comprised of A) 10 mM sodium phosphate dibasic (Na_2HPO_4):10 mM sodium borate ($Na_2B_4O_7$):5 mM sodium azide (NaN_3) and B) 45% Acetonitrile:45% Methanol:10% water. The mobile phase composition achieves separation of each amino acid utilizing a gradient method as shown in Table 2. The flow rate of the mobile phase is 1.5 mL/min. An Agilent AdvanceBio AAA column (4.6 mm x 100 mm, 2.7 µm) was used for analysis at a column temperature of 40.0 °C. To detect the amino acids, a fluorescence detector with an excitation wavelength of 340 nm and emission wavelength of 450 nm is utilized.

Table 1. UHPLC Online Derivatization Steps

Steps	UHPLC Commands
1	Draw 50 µL from borate vial
2	Wait 1 second
3	Draw 2.5 µL from OPA/3-MPA vial
4	Wait 1 second
5	Draw 2.5 µL from borate vial
6	Draw 1.0 µL from sample vial
7	Draw 6.0 µL from air, mix 5 times at default speed
8	Wait 60 seconds
9	Draw 14 µL from injection diluent vial
10	Wait 1 second
11	Draw 15.0 µL from air, mix 5 times at default speed
12	Inject 2 µL

Table 2. Mobile Phase Composition Gradient

Elapsed Time (minutes)	Mobile Phase B
0	2 %
0.35	2 %
13.4	57 %
13.5	100 %
15.7	100 %
15.8	2 %
18	2 %

A sample chromatogram of a multicomponent standard containing 30 µM histidine, tyrosine, and methionine is displayed in Figure 8. Histidine, tyrosine, and methionine elute at 4.16 minutes, 6.47 minutes, and 8.08 minutes, respectively. Table 3 summarizes the free amino acid UHPLC measurement method described above.

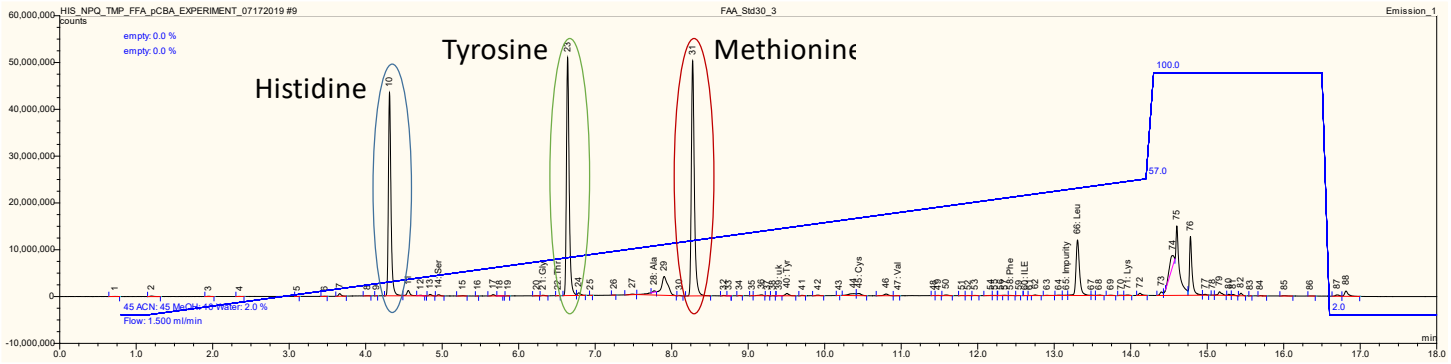

Figure 8. Sample Free Amino Acid Chromatogram

Table 3. Summary of Free Amino Acid UHPLC Measurement

Compound	Analytical Column	Flowrate (mL/min)	Mobile Phase Composition	Excitation Wavelength (nm)	Emission Wavelength (nm)	Injection Volume (µL)	Retention Time (min)	Column Temperature (°C)	Limit of Quantification (µM)
Histidine	Agilent AdvanceBio AAA (4.6 mm x 100 mm, 2.7 µm)	1.5 mL/min	10 mM Na_2HPO_4: 10 mM $Na_2B_4O_7$: 5 mM NaN_3 (pH 8.2)	340	450	2	4.16	40	0.3
Tyrosine			45% MeOH:45% ACN:10% H_2O				6.47		
Methionine							8.08		

2.2.5.2 Furfuryl Alcohol

Furfuryl alcohol is measured using an isocratic mobile phase composition of 60% water: 40% methanol at a flow rate of 1.0 mL/min. An Agilent AdvanceBio AAA column (4.6 mm x 100 mm, 2.7 µm) was used for analysis at a column temperature of 40.0 °C. The sample injection volume was 100 µL detected using a UV-detection wavelength of 220 nm. The retention time of furfuryl alcohol was 1.47 minutes.

2.2.5.3 2,4,6-trimethylphenol

2,4,6-trimethylphenol is measured using an isocratic mobile phase composition of 45% water: 55% methanol at a flow rate of 1.0 mL/min. An Agilent AdvanceBio AAA column (4.6 mm x 100 mm, 2.7 µm) was used for analysis at a column temperature of 40.0 °C. The sample injection volume was 50 µL detected using a UV-detection wavelength of 220 nm. The retention time of 2,4,6-trimethylphenol was 4.47 minutes.

2.2.5.4 Parachlorobenzoic acid

Parachlorobenzoic acid is measured using an isocratic mobile phase composition of 50% water (0.1% phosphoric acid): 50% methanol at a flow rate of 1.0 mL/min. An Agilent AdvanceBio AAA column (4.6 mm x 100 mm, 2.7 µm) was used for analysis at a column temperature of 40.0 °C. The sample injection volume was 50 µL detected using a UV-detection wavelength of 234 nm. The retention time of parachlorobenzoic acid was 4.44 minutes.

2.2.5.5 P-nitroanisole

P-nitroanisole is measured using an isocratic mobile phase composition of 25% water: 75% methanol at a flow rate of 1.0 mL/min. An Agilent AdvanceBio AAA column (4.6 mm x 100 mm, 2.7 µm) was used for analysis at a column temperature of 40.0 °C. The sample injection volume was 50 µL detected using a UV-detection wavelength of 315nm. The retention time of p-nitroanisole was 1.45 minutes. Table 4 below summarizes the measurement of the aforementioned probe compounds.

Table 4. Summary of Probe Compound UHPLC Measurement Methods

Compound	Analytical Column	Flowrate (mL/min)	Mobile Phase Composition	Detection Wavelength (nm)	Injection Volume (µL)	Retention Time (min)	Column Temperature (°C)	Limit of Quantification (µM)
furfuryl alcohol	Agilent AdvanceBio AAA (4.6 mm x 100 mm, 2.7 µm)	1.0 mL/min	60% MQ Water 40% Methanol	220	100	1.47	40	0.4
2,4,6-trimethylphenol			45% MQ Water 55% Methanol	220	50	4.47		0.08
parachlorobenzoic acid			50% MQ Water (0.1% H_3PO_4) 50% Methanol	234	50	4.44		0.19
p-nitroanisole			25% MQ Water 75% Methanol	315	50	1.45		0.095

2.2.6 Estimation of Steady-State Photochemcially Produced Reactive Intermediates (PPRI) using Probe Compounds

In photochemistry, chromophoric dissolved organic matter sensitizes the production of phototechmically produced reactive intermediates (PPRI) such as singlet oxygen ($^1O_2$), hydroxyl radical ($HO^{\bullet}$), and excited triplet state CDOM ($^3CDOM^*$). These PPRI are present at rather low concentrations ($<10^{-10}$ M), so researchers have relied on probe compounds to indirectly estimate the concentrations of these PPRI. For a compound to be used as a probe compound, several criteria must be met. First, probe compounds should

be absolutely selective for the PPRI they are being used to indirectly detect. Second, the probe compound must be stable under photolysis conditions (i.e. not undergo direct phototransformation). Lastly, the probe compound must be miscible in water[1]. Over the next few sections, the derivations for each employed probe compound in this study will be explicated.

2.2.6.1 Steady-State Singlet Oxygen Concentration Estimation using Furfuryl Alcohol

Furfuryl alcohol has been used exclusively to probe the presence of singlet oxygen in numerous photochemical research studies. Schematic 1 below displays the reaction mechanism of furfuryl alcohol with singlet oxygen to produce the three major products. This probe compound relies on the disappearance of furfuryl alcohol.

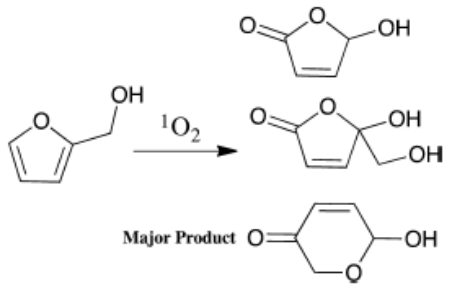

Schematic 1. Furfuryl Alcohol Reaction Mechanism with Singlet Oxygen[27]

Considering this reaction, the reaction rate law would be defined as

$$r_{^1O_2}^{FFA} = \frac{d[FFA]}{dt} = -k_{^1O_2}^{FFA}[FFA][^1O_2] \tag{2.1}$$

Assuming the concentration of $^1O_2$ to be constant allows one to invoke the pseudo-steady state principle. This principle states that the reactive intermediate is short lived and reacts as fast as it is formed, therefore the net rate of formation singlet oxygen is effectively zero.

$$\frac{d[FFA]}{dt} = -k_{^1O_2}^{FFA}[FFA][^1O_2]_{SS} = -k'_{FFA}[FFA] \text{ where } k'_{FFA} = k_{^1O_2}^{FFA}[^1O_2]_{SS} \quad (2.2)$$

Integrating this rate law with respect to time yields,

$$\ln\left(\frac{[FFA]}{[FFA]_0}\right) = -k'_{FFA} \times t \quad (2.3)$$

Plotting the natural-log adjusted concentration of furfuryl alcohol against time yields k', the pseudo-first order observed reaction rate constant. Using this observed rate constant paired with the bimolecular rate constant ($k_{^1O_2}^{FFA}$ = 1 x 10^8 $M^{-1}s^{-1}$) allows the steady-state concentration of singlet oxygen to be estimated.

$$[^1O_2]_{SS} = \frac{k'_{FFA}}{k_{^1O_2}^{FFA}} \quad (2.4)$$

2.2.6.2 Steady-State Excited Triplet State CDOM ($^3CDOM^*$) Concentration Estimation using 2,4,6-trimethylphenol

2,4,6-trimethylphenol (TMP) is an electron rich phenol which reacts selectively with $^3CDOM^*$ as shown in Schematic 2 below.

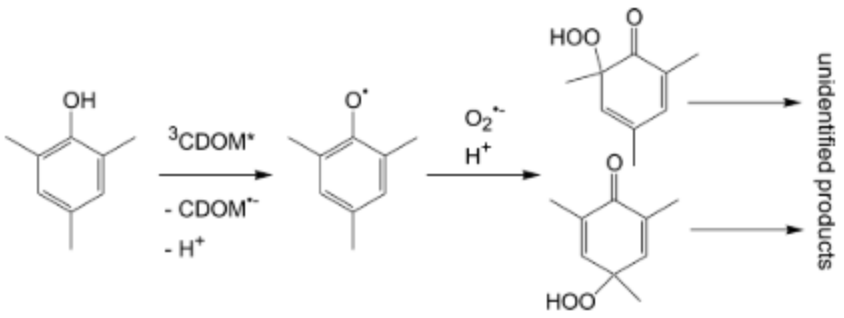

Schematic 2. Reaction Mechanism between 2,4,6-trimethylphenol and ^{3}CDOM*[27]

Considering this reaction, the reaction rate law would be defined as

$$r^{TMP}_{^3CDOOM^*} = \frac{d[TMP]}{dt} = -k^{TMP}_{^3CDOM^*}[TMP][^3CDOM^*] \tag{2.5}$$

Assuming the concentration of ^{3}CDOM* to be constant allows one to invoke the pseudo-steady state principle. This principle states that the reactive intermediate is short lived and reacts as fast as it is formed, therefore the net rate of formation of ^{3}CDOM* is effectively zero.

$$\frac{d[TMP]}{dt} = -k^{TMP}_{^3CDOM^*}[TMP][^3CDOM^*]_{SS} = -k'_{TMP}[TMP] \text{ where } k'_{TMP} = k^{TMP}_{^3CDOM^*}[^3CDOM^*]_{SS} \tag{2.6}$$

Integrating this rate law with respect to time yields,

$$\ln\left(\frac{[TMP]}{[TMP]_0}\right) = -k'_{TMP} \times t \tag{2.7}$$

Plotting the natural-log adjusted concentration of 2,4,6-trimethylphenol against time yields k', the pseudo-first order observed reaction rate constant. Using this observed rate

constant paired with the bimolecular rate constant ($k^{TMP}_{^3CDOM^*}$ = 2 x 10^9 $M^{-1}s^{-1}$) allows the steady-state concentration of excited triplet state CDOM to be estimated.

$$[^3CDOM^*]_{SS} = \frac{k'_{TMP}}{k^{TMP}_{^3CDOM^*}} \tag{2.8}$$

2.2.6.3 Steady-state Hydroxyl Radical (HO•) Concentration Estimating using para-chlorobenzoic acid

Para-chlorobenzoic acid has been used as a probe compound for hydroxyl radical as it reacts selectively as shown in the simplified reaction mechanism in Schematic 3.

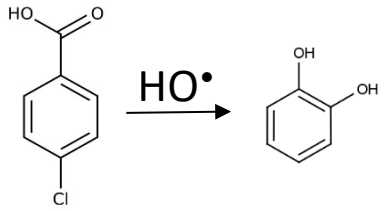

Schematic 3. Parachlorobenzoic Acid Reaction Mechanism with Hydroxyl Radical

Considering this reaction, the reaction rate law would be defined as

$$r^{pCBA}_{HO^\bullet} = \frac{d[pCBA]}{dt} = -k^{pCBA}_{HO^\bullet}[pCBA][HO^\bullet] \tag{2.9}$$

Assuming the concentration of HO• to be constant allows one to invoke the pseudo-steady state principle. This principle states that the reactive intermediate is short lived and reacts as fast as it is formed, therefore the net rate of formation of HO• is effectively zero.

$$\frac{d[pCBA]}{dt} = -k^{pCBA}_{HO^\bullet}[pCBA][HO^\bullet]_{SS} = -k'_{pCBA}[pCBA] \text{ where } k'_{pCBA} = k^{pCBA}_{HO^\bullet}[HO^\bullet]_{SS} \tag{2.10}$$

Integrating this rate law with respect to time yields,

$$\ln\left(\frac{[pCBA]}{[pCBA]_0}\right) = -k'_{pCBA} \times t \tag{2.11}$$

Plotting the natural-log adjusted concentration of parachlorobenzoic acid against time yields k', the pseudo-first order observed reaction rate constant. Using this observed rate constant paired with the bimolecular rate constant ($k_{HO^\bullet}^{pCBA}$ = 2 x 10^9 $M^{-1}s^{-1}$) allows the steady-state concentration of hydroxyl radical to be estimated.

$$[HO^\bullet]_{SS} = \frac{k'_{pCBA}}{k_{HO^\bullet}^{pCBA}} \tag{2.12}$$

2.2.7 Apparent Quantum Yield Derivation

The quantum yield, Φ, is the ratio of decay of a compound, k'_C, to the photolysis rate, k_{abs}:

$$\Phi = \frac{k'_C}{k_{abs}}$$

Furthermore, under the same incident light intensity, the following ratio is maintained:

$$\frac{\Phi_{ref}}{\Phi_{unk}} = \frac{\frac{k'_{ref}}{k_{abs,ref}}}{\frac{k'_{unk}}{k_{abs,unk}}}$$

Where Φ_{ref} is the reference quantum yield of p-nitroanisole, Φ_{unk} is the unknown quantum yield, k'_{ref} is the observed degradation rate of p-nitroanisole from PNA-pyr actinometry, k'_{unk} is the observed degradation rate of the surrogate DOM or the observed degradation rate of furfuryl alcohol for $^1O_2$ quantum yields, $k_{abs,ref}$ is the light absorbance rate constant of p-nitroanisole, and $k_{abs,unk}$ is the light absorbance rate constant of the surrogate DOM.

The light absorbance rate constant (k_{abs}) is a function of the light intensity (I_λ) and the solution molar extinction coefficient (α_λ):

$$k_{abs} = \sum_{\lambda} I_\lambda \alpha_\lambda$$

Rearranging, the unknown quantum yield may be solved for:

$$\Phi_{unk} = \frac{k'_{unk}}{k_{abs,unk}} \frac{k_{abs,ref}}{k'_{ref}} \Phi_{ref}$$

2.2.8 P-nitroanisole –pyridine Actinometry

The p-nitroanisole/pyridine actinometer is a well-characterized visible light actinometer. The actinometer is based on the photodegradation of p-nitroanisole via a reaction between p-nitroanisole and pyridine. The p-nitroanisole reacts with pyridine via pyridine substitution producing p-pyridinium anisole with light ≥ 300 nm as shown in Schematic 4. The pyridine should be in excess, so a pseudo-first order reaction rate can be assumed.

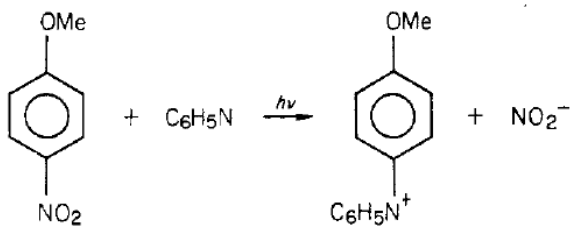

Schematic 4. P-nitroanisole - pyridine Actinometer Reaction[28]

An experimental solution containing a concentration of 10 µM p-nitroanisole and 10 mM pyridine was prepared the morning of the experiment. Experimental solutions were allowed to equilibrate to 20°C. Approximately 50 mL of the experimental solution was transferred to each quartz photoreactor. The SunTest irradiation was set to 500 W/m^2 for this experiment with an acceptable tolerance of +/- 5 W/m^2. The water temperature remained a constant temperature of 20 °C (± 0.3 °C). Photolysis time for this experiment lasted one hour. At each specified time interval, 500 µL aliquots were removed at predetermined time intervals, transferred to autosampler vials, and immediately analyzed on the UHPLC as mentioned in Section 2.2.5.5.

2.2.8.1 PNA-pyr Actinometry Calculations

From the Beer-Lambert Law (eq 2.13), we know that the amount of light absorbed by water is proportional to the concentration of the light absorbing molecules and the path length the light takes in passing through the water.

$$A(\lambda) = \log\left(\frac{I}{I_0}\right) = -\varepsilon_\lambda \cdot C \cdot l \qquad (2.13)$$

$$I = I_{0,\lambda}\left(10^{-\varepsilon_\lambda \cdot C \cdot l}\right) \qquad (2.14)$$

$$I_A = I_{0,\lambda}\left(1-10^{-\varepsilon_\lambda \cdot C \cdot l}\right) \qquad (2.15)$$

Where A(λ) is the absorbance (dimensionless), I is the intensity of light passing through the sample at each wavelength, I_0 is the overall intensity hitting the top of the solution, ε_λ is the molar extinction coefficient at each wavelength ($M^{-1}cm^{-1}$) , C is the concentration of the light absorbing molecules (M), and l is the light path length (cm).

Combining this knowledge with our known knowledge of quantum yield or the fraction of absorbed photons that result in a photolysis reaction, one may begin to relate the equations to determine the overall photon fluence rate.

$$\text{Quantum yield } (\Phi_\lambda, \frac{mol}{einstein}) = \frac{-r_r}{I_A} = \frac{\text{photolysis reaction rate}}{\text{photon absorption rate}} = \frac{\left(\frac{mol}{L-s}\right)}{\left(\frac{einstein}{1000\ cm^3 - s}\right)} \qquad (2.16)$$

Substituting eq 1.3 into eq 1.4, we obtain

$$\Phi_\lambda = \frac{-r_r}{I_{0,\lambda}\left(1-10^{-\varepsilon_\lambda \cdot C \cdot l}\right)\cdot 1000} = \frac{k'[C_0]}{1000 \cdot \sum_{800nm}^{300nm} I_{0,\lambda}\left(1-10^{-\varepsilon_\lambda \cdot C_0 \cdot l}\right)\Delta\lambda} \qquad (2.17)$$

Now, let's normalize the photon fluence rate at each wavelength using eq 1.6:

$$\rho_\lambda = \frac{E^0_{p_\lambda}}{\sum_{800nm}^{300nm} E^0_{p_\lambda}\Delta\lambda} = \frac{E^0_{p_\lambda}}{E^0_{\rho,tot}} \qquad (2.18)$$

Substituting the normalized photon fluence rate into the denominator of eq.1.5 yields:

$$\Phi_\lambda = \frac{k'[C_0]}{1000 \cdot \frac{1}{l} \sum_{800nm}^{300nm} \rho_\lambda \left(1 - 10^{-\varepsilon_\lambda \cdot C_0 \cdot l}\right) \Delta\lambda} \tag{2.19}$$

Now, rearranging eq. 1.6 to solve for the total photon fluence rate:

$$E^0_{\rho,tot} = \frac{k'[PNA_0]l}{1000 \cdot \Phi \cdot \sum_{800nm}^{300nm} \rho_\lambda \left(1 - 10^{-\varepsilon_\lambda \cdot [PNA_0] \cdot l}\right) \Delta\lambda} \tag{2.20}$$

Where k' is the pseudo-first order reaction rate constant (1/s), $[PNA_0]$ is the initial concentration of p-nitroanisole (typically 10 μM), and Φ_{PNA} is the quantum yield of p-nitroanisole estimated from Laszakovitz et al. (2017)'s experimentally determined correlation of $\Phi_{PNA} = 0.29[pyr] + 0.00029$[29].

2.2.9 Surrogate DOM Photolysis Transformation Calculations

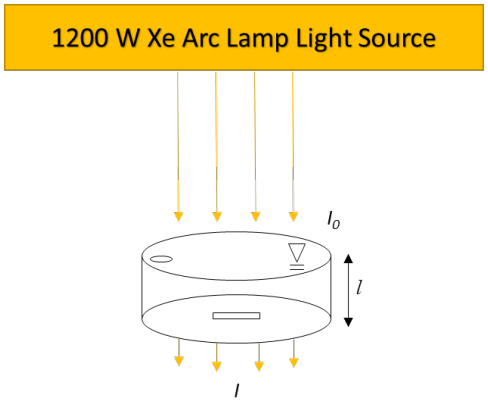

where,

I_0 = photon intensity at surface of reactor (einstein/cm^2-s)

I = photon intensity after passing through solution containing water constituents at wavelength λ (einstein/cm^2-s)

l = depth of photoreactor

C = concentration (mole/L)

$\varepsilon'(\lambda)$ = base-e extinction coefficient (L/mol/cm)

where I_a = volumetric photon absorption rate (einstein/cm^3-s)

Definition of Quantum Yield

$$\phi(\lambda) = \frac{-r}{I_a}$$

where

Φ(λ) = quantum yield at wavelength λ (mole/einstein)

r = reaction rate (mole/cm^3-s)

I_a = volumetric photon absorption rate (einstein/cm^3-s)

$$r = -\Phi(\lambda) I_a$$

$$= -\Phi(\lambda) \cdot I_0 \cdot \varepsilon'(\lambda) \cdot C \cdot e^{-\varepsilon'(\lambda)Cl}$$

$$r_{avg} = \frac{1}{l}\int_0^l r \cdot dx$$

$$r_{avg} = -\frac{1}{l}\int_0^l -\Phi(\lambda) \cdot I_0 \cdot C \cdot e^{-\varepsilon'(\lambda)Cl} dx$$

$$r_{avg} = -\frac{\Phi(\lambda) \cdot I_0 \cdot \varepsilon'(\lambda) \cdot C}{l}\left(-\frac{1}{\varepsilon'(\lambda) \cdot C}\right)\left[e^{-\varepsilon'(\lambda)Cl} - 1\right]_0^l$$

$$r_{avg} = \frac{\Phi(\lambda) \cdot I_0}{l}\left[e^{-\varepsilon'(\lambda)Cl} - 1\right]$$

$$r_{avg} = \frac{-\Phi(\lambda) \cdot I_0}{l}\left[1 - e^{-\varepsilon'(\lambda)Cl}\right]$$

$$P_{U-V} = \frac{I_0}{l} = \text{ photonic intensity } \left(\frac{einstein}{cm^3 \cdot s}\right)$$

$$r_{avg} = -\Phi(\lambda) \cdot P_{U-V}\left[1 - e^{-\varepsilon'(\lambda)Cl}\right] \qquad (1.1)$$

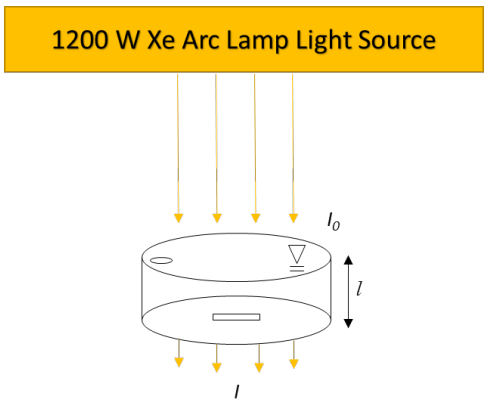

where,

I_0 = photon intensity at surface of reactor (einstein/cm^2-s)

I = photon intensity after passing through solution containing water constituents at wavelength λ (einstein/cm^2-s)

l = depth of photoreactor

C = concentration (mole/L)

ε'(λ) = base-e extinction coefficient (L/mol/cm)

$$
\begin{aligned}
I &= \int_0^l I_0 e^{-\varepsilon'(\lambda)x} dx \\
&= -I_0 \frac{1}{\varepsilon'(\lambda)} \left[e^{-\varepsilon'(\lambda)x} \right]_0^l \\
&= -\frac{I_0}{\varepsilon'(\lambda)} \left[e^{-\varepsilon'(\lambda)l} - 1 \right] \\
&= -\frac{I_0}{\varepsilon'(\lambda)} e^{-\varepsilon'(\lambda)l} + \frac{I_0}{\varepsilon'(\lambda)} \\
I &= I_0 \left[\frac{1}{\varepsilon'(\lambda)} - \frac{e^{-\varepsilon'(\lambda)l}}{\varepsilon'(\lambda)} \right]
\end{aligned}
$$

$$
I_0 = \frac{I}{\frac{1}{\varepsilon'(\lambda)} - \frac{e^{-\varepsilon'(\lambda)l}}{\varepsilon'(\lambda)}} \tag{1.2}
$$

Plugging eqn. 1.2 into eqn. 1.1 yields, the zeroth-order rate for the surrogate DOM transformation.

$$
r = -\frac{\Phi(\lambda)}{l} \frac{I}{\frac{1}{\varepsilon'(\lambda)} - \frac{e^{-\varepsilon'(\lambda)l}}{\varepsilon'(\lambda)}} \left\{ 1 - e^{-\varepsilon'(\lambda)Cl} \right\} \tag{1.3}
$$

Looking at equation 1.3, all information is known about our surrogate DOM and photolysis with the exception of the quantum yield. The molar absorptivity coefficient, ε'(λ), was measured using a spectrophotometer, the depth of solution is 2 cm, and I is the measured photon flux in Einstein/L-s.

The quantum yield of the surrogate DOM, Φ(λ), may be estimated using the apparent quantum yield as described by Remucal and McNeill (2011)[14].

$$\Phi_{unk} = \frac{k_{obs}^{DOM}}{k_{obs}^{std}} \frac{k_{abs}^{std}}{k_{abs}^{DOM}} \Phi_{std} \tag{1.4}$$

Where k_{obs}^{DOM} is the observed degradation rate of the surrogate DOM, k_{obs}^{std} is the observed degradation rate of the PNA-pyr actinometer, k_{abs}^{std} is the light absorbance rate constant for PNA-pyr actinometry, and k_{abs}^{DOM} is the light absorbance rate constant for surrogate DOM.

$$k_{abs} = \sum_{280\text{ nm}}^{800\text{ nm}} I_\lambda \varepsilon'(\lambda) \tag{1.5}$$

Where, I_λ is the measured light intensity from a spectroradiometer (einsteins/L-s) and ε'(λ) is the base-e molar absorptivity coefficient, both in the range of 280 nm to 800

3 Results and Discussion

3.1 Overall results

The direct photolysis of free amino acids was confirmed to be negligible due to the little absorbance of photons by our free amino acids in 290-800 nm wavelength (Figure 9), which is consistent with findings in the literature.[6, 14-16] Thus, all the decays of free amino acids are due to the reactions with PPRIs sensitized by DOM which had varying degrees of absorbance in the 290-800 nm wavelength range (Figure 10).

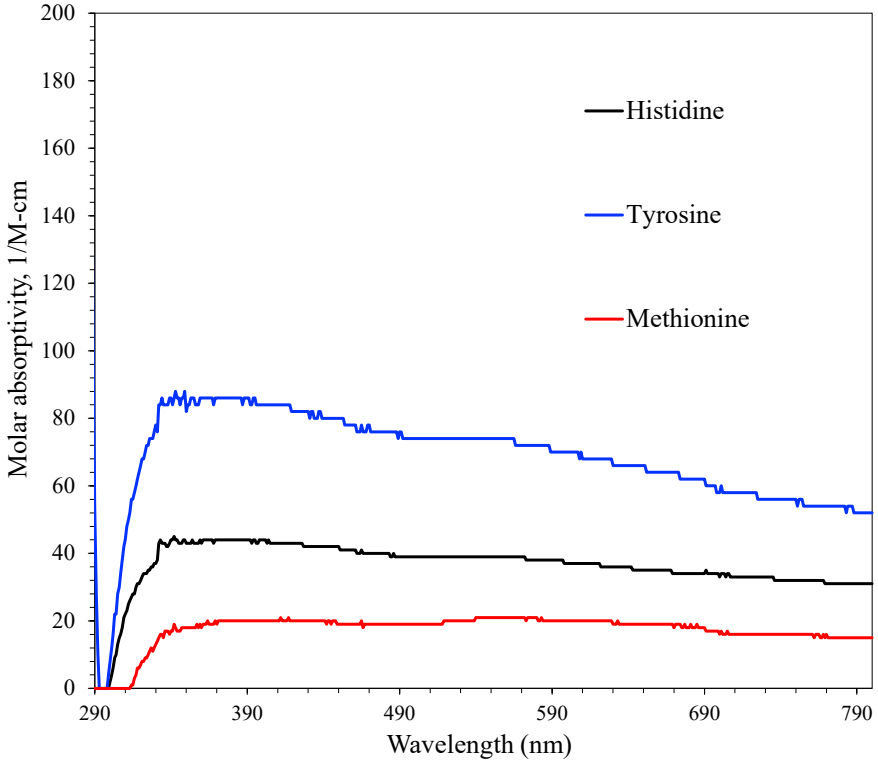

Figure 9: Free Amino Acid Molar Absorptivity in UV-Vis Range

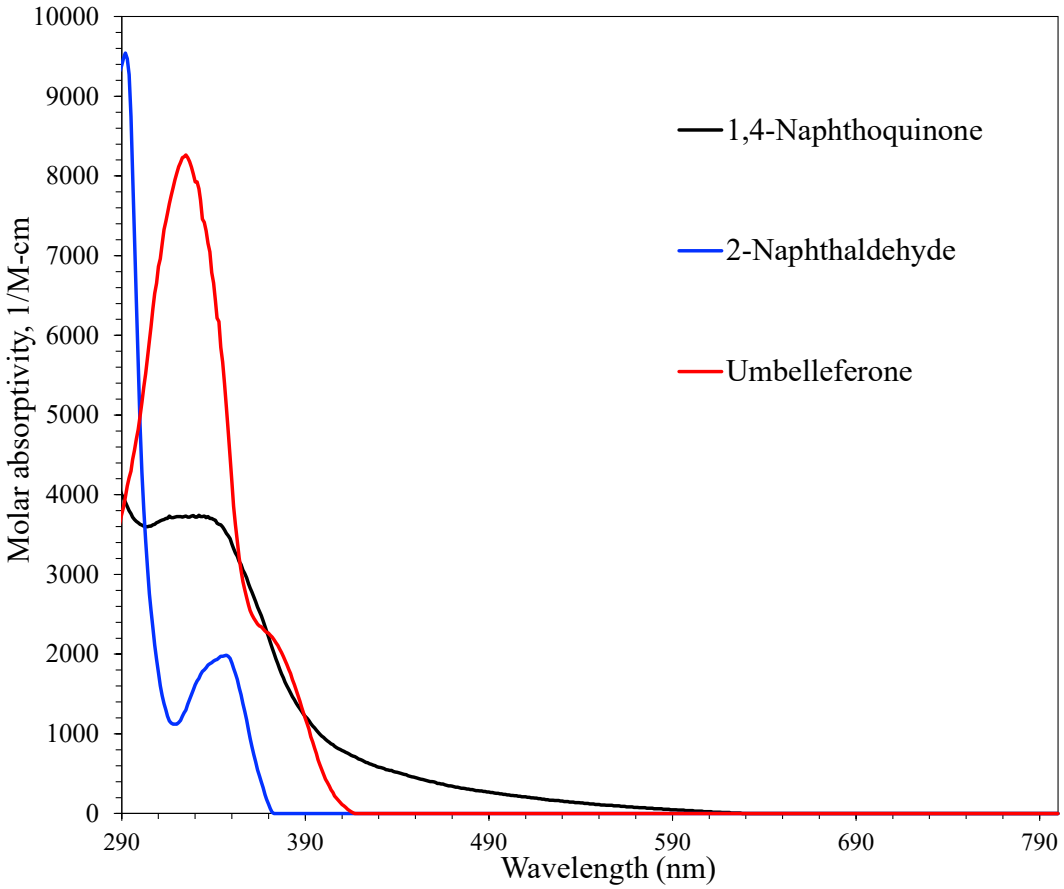

Figure 10: Surrogate DOM Molar Absorptivity in UV-Vis Range

Figure 12 represents the pseudo-first order decay of three amino acids at three solution temperatures in the presence of three surrogate DOM and natural organic matter isolate SRNOM. While we obtained the linear relationships between $\ln(C/C_0)$ and the reaction time, those obtained in the presence of 1,4-naphthoquinone did not apparently follow this relationship. To clarify the nature of the pseudo-first order kinetics law, we examined the time-dependent profile of chromophores of our surrogate DOM (the detailed analysis is given in Section 2.2.8 and Figure 10). Though 1,4-naphthoquinone and 2-naphthaldehyde are both present in many DOM isolates, their structure is quite different. 1,4-naphthoquinone is a naphthalene ring with two substituted carbonyl

moieties (i.e. quinone). These carbonyl groups absorb most strongly near the UV-vis range around 275 nm. The combining effect of C=O and C=C leads to the most widespread absorbance of all surrogate DOM in this study from 300 to 600 nm and explains its ability to sensitize a wide range of PPRI. On the other hand, 2-naphthaldehyde is a naphthalene ring substituted with a formyl group at position 2. The C=C bonds and C=O lead to strong absorption below 400 nm.

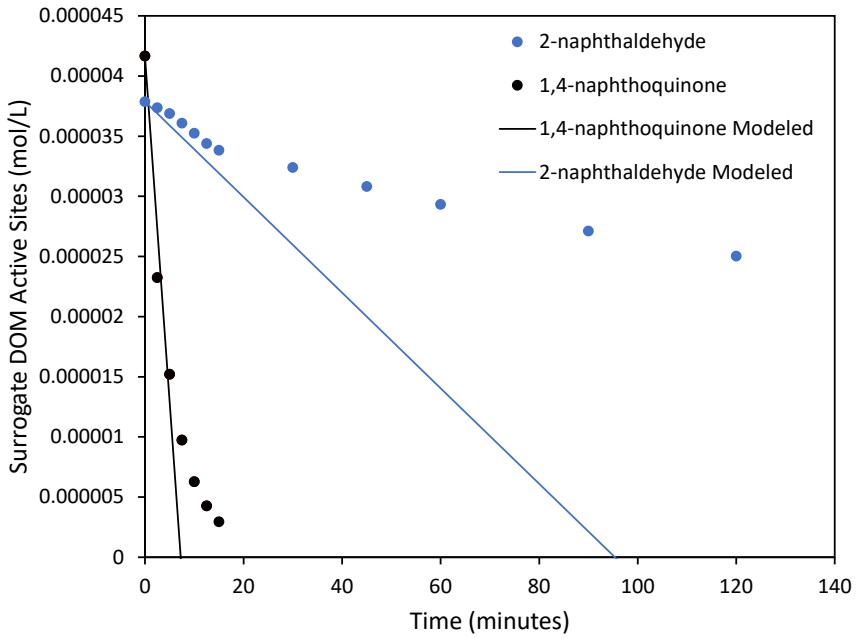

Figure 11: Surrogate DOM Experimental and Calculated Phototransformation

While the chromophoric component of 2-naphthaldehyde was available over the reaction time, that of 1,4-naphthoquinone disappeared quickly within the initial 20 minutes of the photolysis reaction time (Figure 11). While molar absorptivity of our three surrogate DOM over 290-800 nm are comparable (Figure 10), high quantum yield of 1,4-naphthoquinone results in the initial phototransformation and complete disappearance of

the chromophores. The 1,4-naphthoquinone triplet has a high tendency to undergo hydration in the presence of water leading to its fast degradation[21]. The calculated decay rate of both 1,4-naphthoquinone and 2-naphthaldehyde is consistent with those of chromatographic decay verifying the initial fate of 1,4-naphthoquinone. Accordingly, the analysis of free amino acids and probe compounds in the presence of 1,4-naphthoquinone was conducted in two phases: (1) Phase 1 where quinone is in charge of absorbing photon up to 15 minutes of reaction time and (2) Phase 2 where resultant of 1,4-naphthoquinone and transformed structure are in charge of absorbing photons and excitation from 15 minutes to 120 minutes of reaction time. Additionally, umbelliferone did not sensitize any PPRI, so its analysis regarding the degradation of probe compounds and free amino acids is excluded. To probe the inertness of umbelliferone, it is critical to examine the physicochemical attributes of coumarins such as umbelliferone. Schematic 5 below displays the activation pathway of chromophoric dissolved organic matter. Ground state CDOM absorbs photons from sunlight exciting the CDOM to its singlet excited state, $^{1}CDOM^{*}$. Once in this state, it may relax back to its ground state or undergo intersystem crossing whose efficiency is determined by the quantum yield, Φ_{ISC}, its excited triplet state, $^{3}CDOM^{*}$. In its triplet state, CDOM may relax, be quenched by $^{3}O_2$, or react with $^{3}O_2$. Between $^{3}CDOM^{*}$ and $^{3}O_2$, the fraction of reactions that lead to $^{1}O_2$, f_{Δ} and the fractions that are quenched, $1\text{-}f_{\Delta}$. As singlet oxygen, these reactions may relax to ground state oxygen or continue to undergo transformation with other substrates leading to the formation of the hydroxyl radical and hydrogen peroxide or transformation of organic compounds.

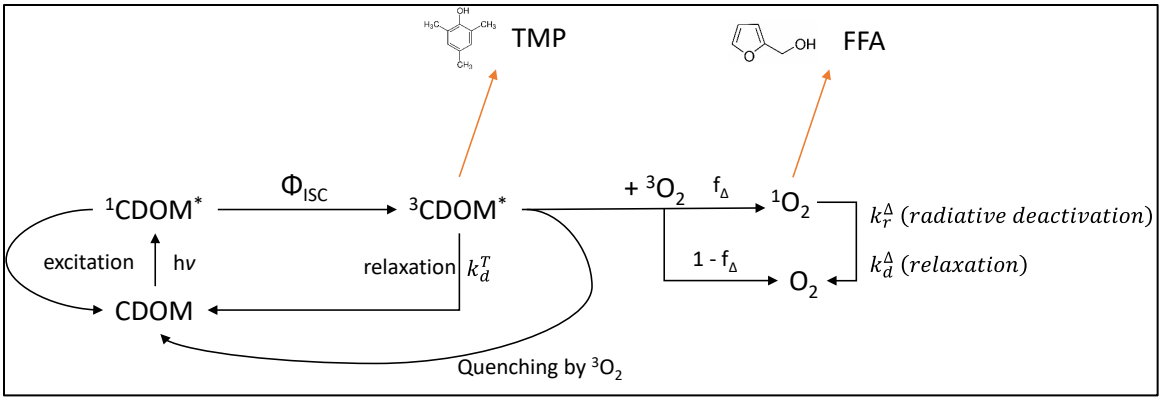

Schematic 5: Simplified Schematic for the Sensitization of CDOM

In general, coumarins such as umbelliferone have been shown to have very low intersystem crossing ($0.1 < \Phi_{ISC} < 0.4$)[30-36] from their singlet state to triplet state. In umbelliferone's excited singlet state, its relaxation to ground state may undergo several pathways. Umbelliferone has a very low fluorescence quantum yield below 0.08 indicating its insignificance to its relaxation[30, 33]. The major pathway for relaxation is through excited-state proton transfer with a rate constant of 2×10^{10} s^{-1} meaning it accepts an excess proton from weak acids in solution[32, 35, 36] This extremely fast relaxation to ground state from its excited singlet state explains its insignificant role in degrading the free amino acids

The solution temperature significantly affected the decay of all free amino acids in the presence of all surrogate DOM. The temperature-dependent pseudo-first order rate constant of each amino acid in the presence of the surrogate DOM are displayed in Table 5. Over the initial 15 minutes of reaction time with 1,4-naphthoquinone, histidine and methionine react nearly 3 times and 1.5 times higher degradation with an increase in temperature from 10 °C to 30 °C, respectively; conversely, tyrosine shows minimal

dependence on temperature. Over the second phase of the reaction time, histidine and methionine also show higher degradation with an increase in temperature, though at a rate 12-18 times slower than the first phase. Again, tyrosine's degradation is minimal over the second phase. Using the temperature dependent pseudo-first order rate constants (Table 1), the activation energy of each amino acids' decay in the presence of 2-naphthaldehyde and 1,4-naphthoquinone may be estimated by plotting ln(k) vs. 1/Temperature (K) (Figure 13). With 1,4-naphthoquinone, tyrosine has the lowest activation energy of 0.49 kcal/mol, followed by methionine (3.79 kcal/mol), then histidine (7.80 kcal/mol) indicating that histidine is most susceptible to temperature change.

In this initial 15 minutes, 1,4-naphthoquinone undergoes significant phototransformation. Once promoted to its triplet state, 1,4-naphthoquinone undergoes three major pathways: (1) relax to its ground state; (2) react with water producing quinone-H_2O adducts[21, 37, 38]; and (3) react with target amino acid[6, 14-17, 39, 40]. Kinetically, pathway 3 ($\sim 10^9$ M^{-1} s^{-1}) is the most favorable followed by pathway 2 (2.25×10^6 s^{-1}), though the availability of water is much higher than the availability of amino acid, which leads to 1,4-naphthoquinone's quick disappearance in the initial phase of the photolysis reaction. This hydration reaction yields several stable photoproducts – 1,4 dihydroxynaphthalene and 5- and 7-hydroxy-1,4-naphthoquinone - which are prominent in the second phase of the photolysis leading to the slow decay of the free amino acids[21].

In contrast, with 2-naphthaldehyde, histidine, tyrosine, and methionine all show higher degradation with increased solution temperature. Histidine's rate doubles from 10 °C to 30 °C, tyrosine's rate is nearly 20 times higher from 10 °C to 30 °C, and

methionine's rate is about 1.5 times higher over the same temperature increase. In the presence of 2-naphthaldehyde, methionine is least susceptible to temperature change with an activation energy of 4.36 kcal/mol, followed by histidine (5.86 kcal/mol), and finally tyrosine (26.15 kcal/mol).

In the presence of SRHA, the amino acids followed pseudo-first order kinetics degrading in the following order: Histidine > tyrosine > methionine which has been confirmed by previous studies.[6]

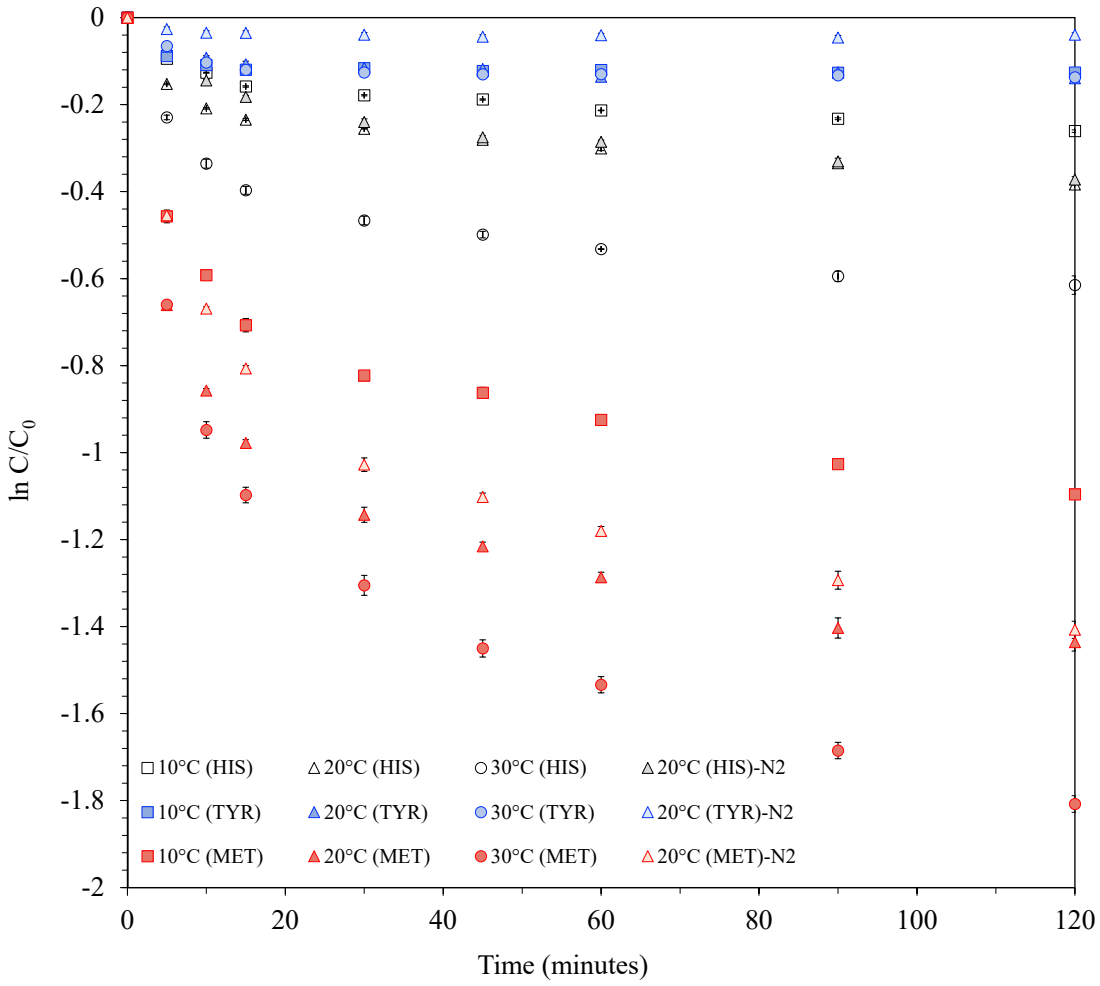
0
-0.2
-0.4
-0.6
-0.8
-1
-1.2
-1.4
-1.6
-1.8
-2
ln C/C0
0
20
40
60
80
100
120
Time (minutes)
10°C (HIS)
20°C (HIS)
30°C (HIS)
20°C (HIS)-N2
10°C (TYR)
20°C (TYR)
30°C (TYR)
20°C (TYR)-N2
10°C (MET)
20°C (MET)
30°C (MET)
20°C (MET)-N2

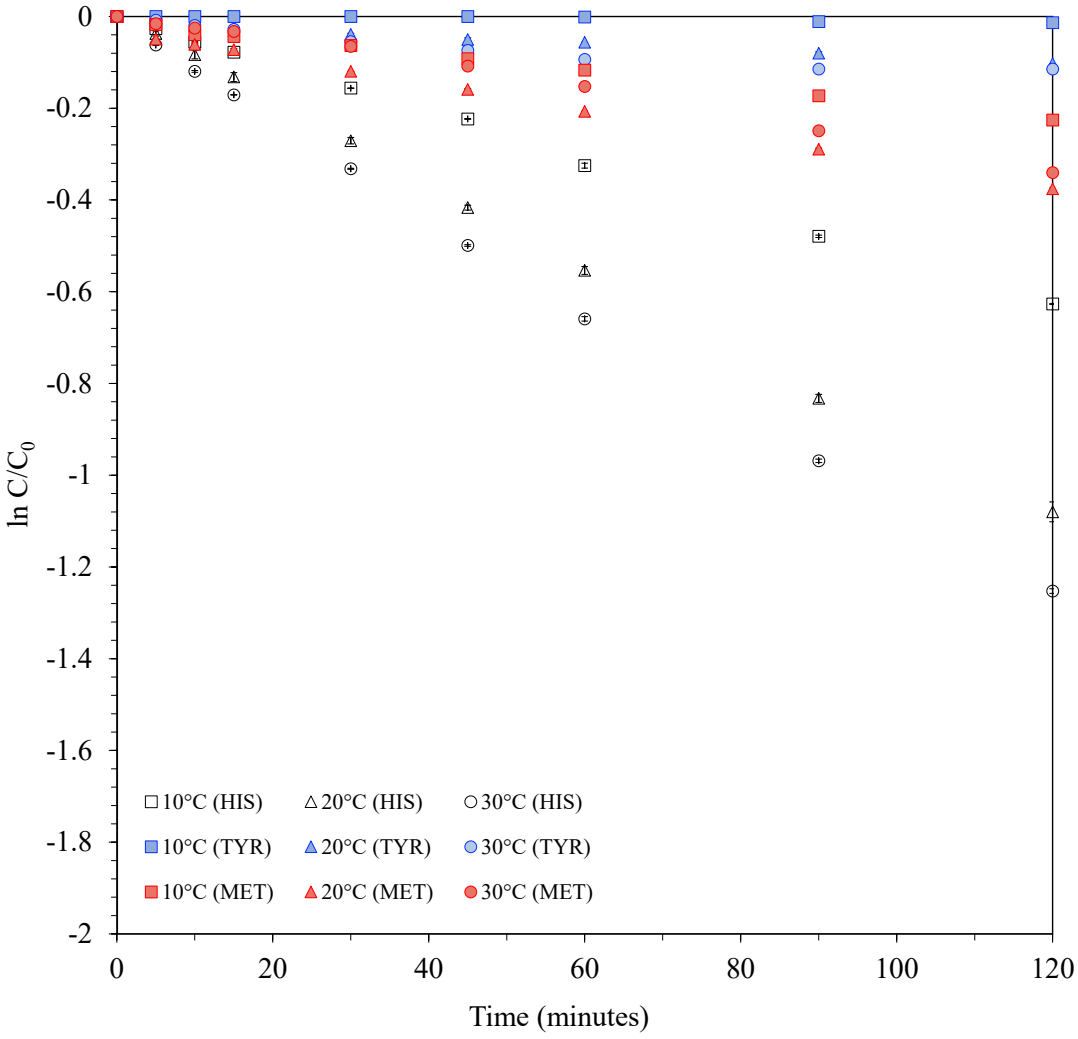
0
-0.2
-0.4
-0.6
-0.8
-1
-1.2
-1.4
-1.6
-1.8
-2
ln C/C0
0
20
40
60
80
100
120
Time (minutes)
10°C (HIS)
20°C (HIS)
30°C (HIS)
10°C (TYR)
20°C (TYR)
30°C (TYR)
10°C (MET)
20°C (MET)
30°C (MET)

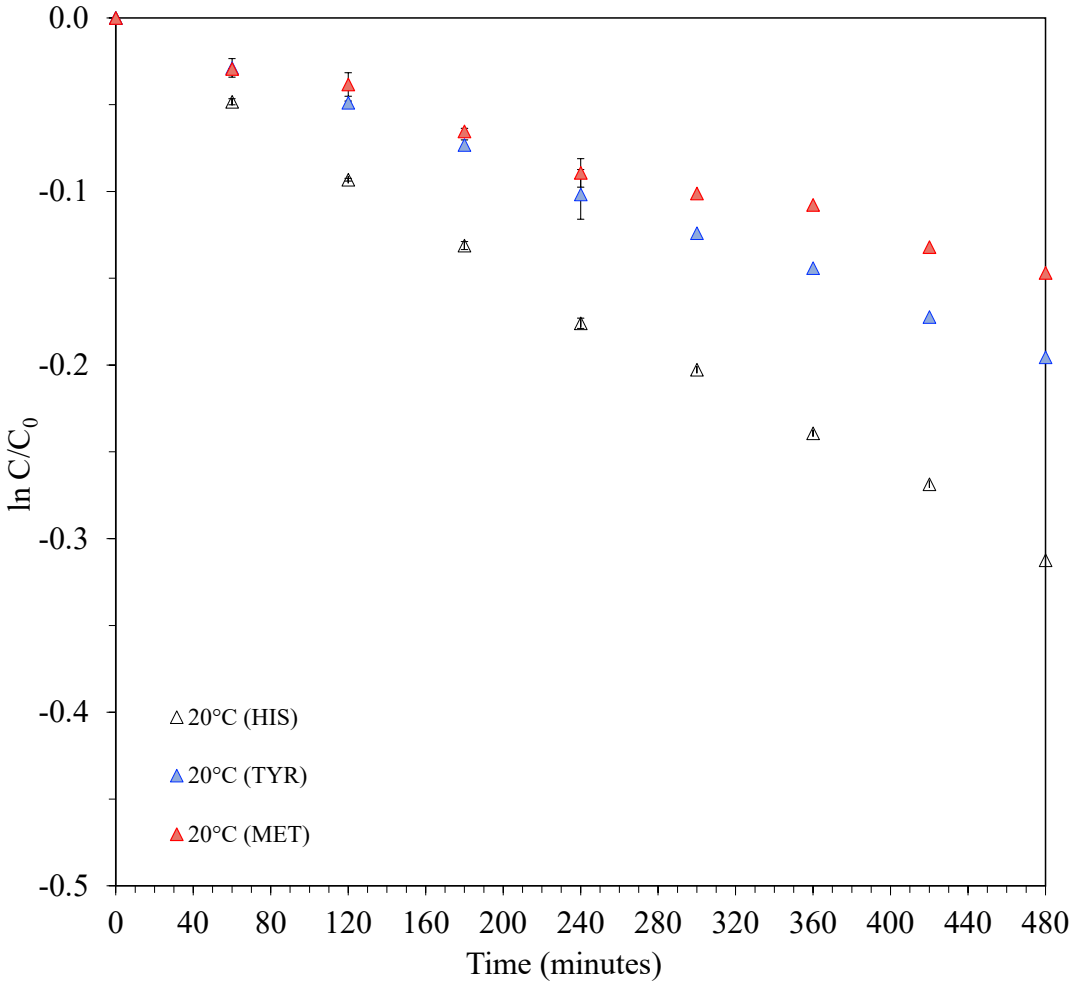

Figure 12: A natural log-plot of concentration profiles of each free amino acid over time at three different temperatures in the presence of: 1,4-naphthoquinone (top), 2-naphthaldehyde (middle), and Suwannee River Humic Acid (bottom). Error bars are the standard deviation of each measurement.

Table 5: Pseudo-first order decay rate constants of three amino acids in the presence of three surrogate DOM at three different temperatures

	1,4-Naphthoquinone						2-Naphthaldehyde			Umbelliferone		
	First phase			Second phase								
	Histidine	Tyrosine	Methionine	Histidine	Tyrosine	Methionine	Histidine	Tyrosine	Methionine	Histidine	Tyrosine	Methionine
10°C	-0.012	-0.0095	-0.054	-0.0010	-0.00009	-0.0035	-0.0053	-0.00009	-0.0019	n.a.	n.a.	n.a.
20°C	-0.018	-0.0082	-0.076	-0.0014	-0.00027	-0.0041	-0.0091	-0.0009	-0.0033	-0.00055	negligible	-0.00078
20 with N_2	-0.013	-0.0029	-0.060	-0.0017	-0.00004	-0.0052	n.a.	n.a.	n.a.	n.a.	n.a.	n.a.
30°C	-0.030	-0.0090	-0.084	-0.0020	-0.00014	-0.0064	-0.0107	-0.0019	-0.0027	n.a.	n.a.	n.a.

Comparing the pseudo-first order rate constants between the surrogate DOM and DOM isolate (i.e., SRHA) at 20°C, histidine's pseudo-first order rate constant in the presence of 1,4-naphthoquinone (0.018 min^{-1}) is double that with 2-naphthaldehyde (0.0091 min^{-1}) and 25 times that with SRHA (0.0007 min^{-1}). Tyrosine's pseudo-first order rate constant in the presence of 1,4-naphthoquinone (0.0082 min^{-1}) is 9 times higher than with 2-naphthaldehyde (0.0009 min^{-1}) and 20 times higher with SRHA (0.0004 min^{-1}). Methionine's pseudo-first order rate constant in the presence of 1,4-naphthoquinone (0.076 min^{-1}) is 23 times higher than with 2-naphthaldehyde (0.0033 min^{-1}) and 250 times higher than with SRHA (0.0003 min^{-1}). It is important to consider the differences in pseudo-first order reaction rate constants between DOM isolates and surrogate DOM. The differences in reactivity stem from the high concentrations of pure surrogate DOM as mg C/L in comparison to SRHA's composition which has much lower concentrations of many different critical sensitizers such as quinones, ketones, aldehydes, coumarins, and aromatic hydrocarbons[26, 41]. Though these solutions containing pure surrogate DOM are not representative of the natural environment, the reactions between our surrogate DOM and FAA provide mechanistic insights into the transformation of SRHA. Comparing these results to the surrogate DOM, it is important to notice the difference in both the

time and log-adjusted scales. For a fraction of the free amino acid photodegradation, the amino acids were photolyzed for four times longer with SRHA than in the presence of the surrogate DOM.

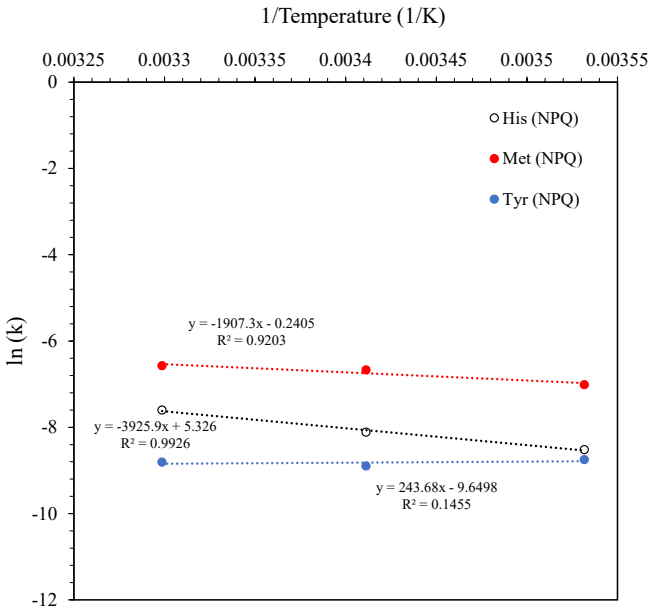

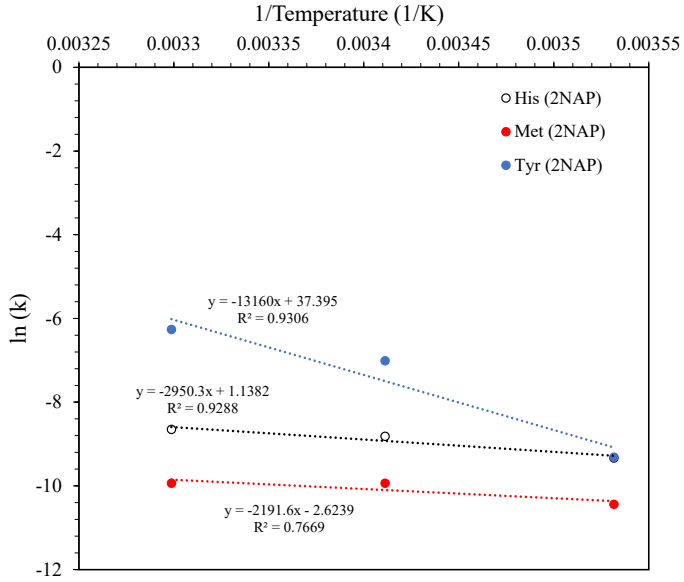

Figure 13: A natural log-plot of pseudo-first order rate constant of each free amino acid vs. the inverse of the temperature (1/K) in the presence of: 1,4-naphthoquinone (top), 2-naphthaldehyde (bottom).

3.2 Contributions of PPRIs to each free amino decay

To investigate the temperature-dependent contribution of each PPRI to the free amino acid decay, several well-studied probe compounds including furfuryl alcohol[27, 40, 42], 2,4,6-trimethylphenol[22, 27, 43-46], and parachlorobenzoic acid[13, 47] were employed. Figure 14 shows the temperature-dependent probe compound degradation profiles in the presence of each surrogate DOM. Of all the probe compounds, 1,4-naphthoquinone degrades furfuryl alcohol the fastest, followed by TMP, then pCBA indicating that it sensitizes all PPRI (i.e., $^1O_2$, $^3CDOM^*$, $HO^\bullet$). 2-naphthaldehyde degrades TMP most rapidly, followed by furfuryl alcohol, while pCBA is inert with it. The triplet energies – amount of energy transferred during reaction - of 1,4-naphthoquinone and 2-naphthaldehyde are 57.6 kcal/mol and 59.5 kcal/mol[26], respectively. Using TMP as an indicator for $^3CDOM^*$, it is evident that 2-naphthaldehyde sensitizes $^3CDOM^*$ very efficiently leading to its strong oxidation and rapid consumption of TMP in the initial 15 minutes, which is reflective of its high triplet energy.

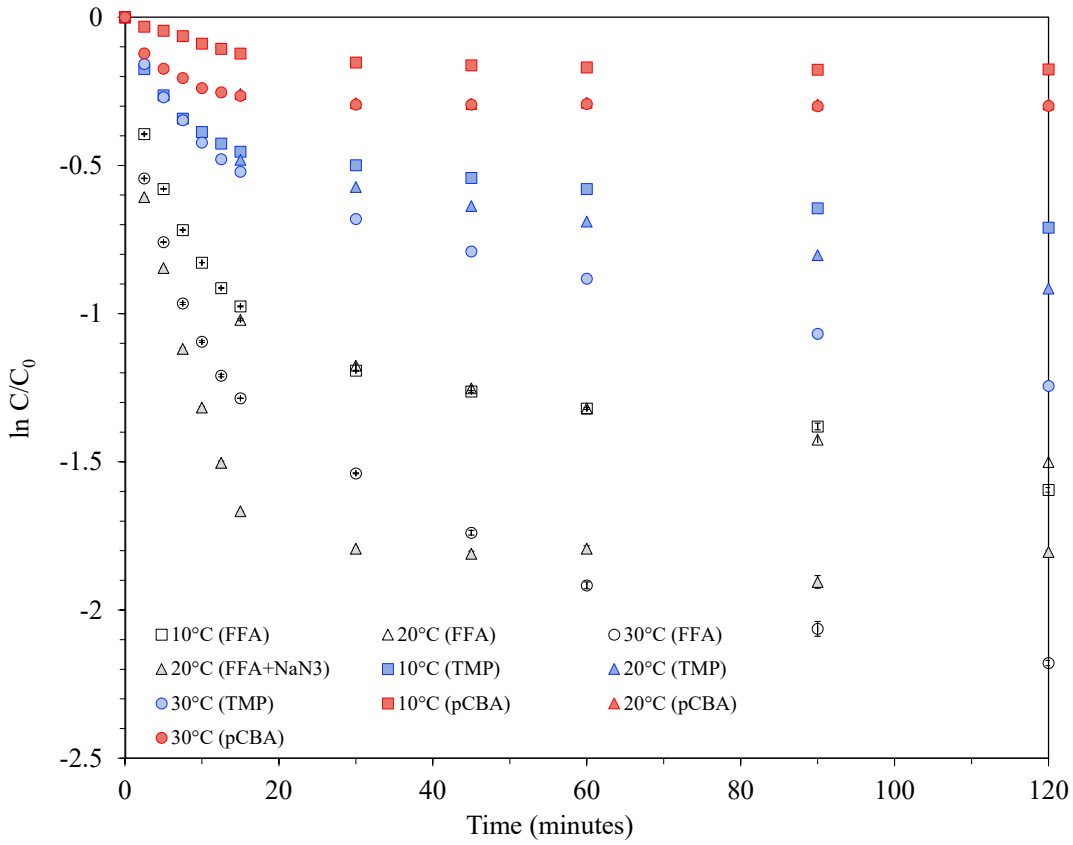
0
-0.5
-1
-1.5
-2
-2.5
ln C/C0
0
20
40
60
80
100
120
Time (minutes)
10°C (FFA)
20°C (FFA)
30°C (FFA)
20°C (FFA+NaN3)
10°C (TMP)
20°C (TMP)
30°C (TMP)
10°C (pCBA)
20°C (pCBA)
30°C (pCBA)

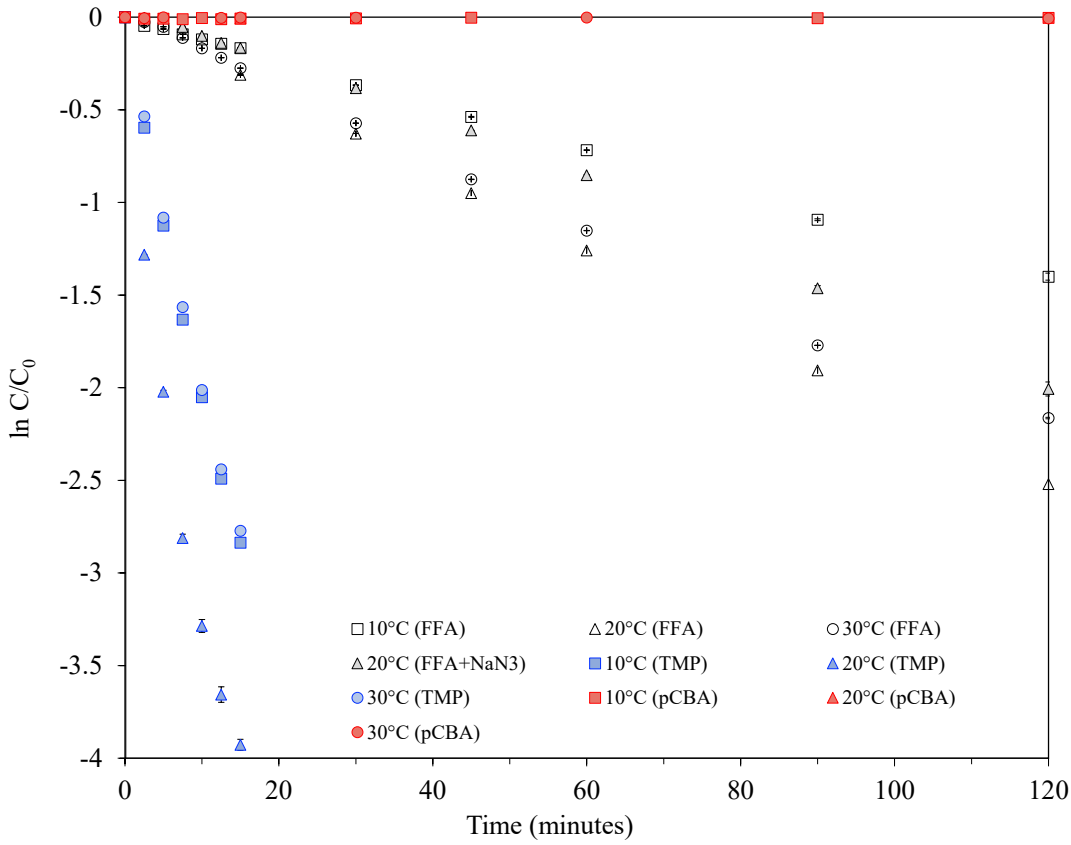

Figure 14: A natural log-plot of concentration profiles of FFA, TMP, and pCBA over time at three different temperatures in the presence of: 1,4-naphthoquinone (top) and 2-naphthaldehyde (bottom). Error bars are each measurement's standard deviation.

From these probe compound photolysis degradation profile, the temperature-dependent apparent quantum yields for singlet oxygen, excited triplet state CDOM, and hydroxyl radical were calculated[14, 40, 43] and displayed in Table 6. To estimate the apparent quantum yield, the surrogate DOM triplet states' rate constants with TMP and $^3O_2$ were estimated using Rehm-Weller relationships previously developed[48, 49]. 1,4-naphthoquinone's triplet state bimolecular rate constant with TMP and $^3O_2$ are estimated as 4-5 × 10^9 M^{-1} s^{-1} and 3× 10^{10} M^{-1} s^{-1}. 2-naphthaldehyde's triplet state bimolecular rate

constant with TMP and $^3O_2$ are estimated as 1-4 × 10^9 M^{-1} s^{-1} and 1.6 × 10^9 M^{-1} s^{-1}, respectively.

Table 6: Quantum yield of each PPRI in the presence of three surrogate DOM at three different temperatures

	1,4-Naphthoquinone						2-Naphthaldehyde			Umbelliferone		
	First phase			Second phase								
	$^1O_2$	^{3}DOM*	HO*	$^1O_2$	^{3}DOM*	**HO•**	$^1O_2$	^{3}DOM*	HO*	$^1O_2$	^{3}DOM*	**HO•**
10°C	0.194	0.0904	0.0215	0.0109	0.0061	0.001	0.189	4.807	n.a.	n.a.	n.a.	n.a.
20°C	0.172	0.0813	0.0438	0.0127	0.0101	0.0005	0.336	3.175	n.a.	0.0035	0.004	negligible
20 with NaN	0.257	n.a.	n.a.	0.003	n.a.	n.a.	0.251	n.a.	n.a.	n.a.	n.a.	n.a.
30°C	0.317	0.0995	0.0544	0.0208	0.017	0.0005	0.297	3.095	n.a.	n.a.	n.a.	n.a.

At 20 °C, 1,4-naphthoquinone sensitizes $^1O_2$ most efficiently at twice the factor of $^3CDOM^*$ and 4 times that of $HO^\bullet$ which is consistent with other studies[21, 37]. Additionally, with an increasing solution temperature, all PPRI quantum yields increased in both the first and second phase. With 2-naphthaldehyde, $^3CDOM^*$ quantum yields are significantly higher than 1,4-naphthoquinone over all temperatures, whereas $^1O_2$ quantum yields are comparable to 1,4-naphthoquinone. Both singlet oxygen apparent quantum yields are comparable to other studies[26, 50, 51]. Interestingly, 2-naphthaldehyde's singlet oxygen apparent quantum yields increase with increasing temperature, though its $^3CDOM^*$ quantum yield decreases. This indicates that intersystem crossing may be inhibited at higher temperatures, though the charge transfer from $^3CDOM^*$ to oxygen is accelerated to produce greater $^1O_2$ concentrations.

Table 7: Calculated Activation Energy (kcal/mol) of each Free Amino Acid Reaction Pathway

	Histidine	Tyrosine	Methionine
ΔG^{act}_{SET} (^{3}DOM*, 1,4-Naphthoquinone)	3.2	8.5	1.6
ΔG^{act}_{SET} (^{3}DOM*, 2-Naphthaldehyde)	15.3	19.0	19.8
ΔG^{act}_{SET} (^{3}DOM*, Umbelliferone)	12.1	14.7	16.1
ΔG^{act}_{SET} ($^1O_2$)	15.6	16.5	18.8
ΔG^{act}_{SET} (HO*)	13.7	21.1	19.0
ΔG^{act}_{add} ($^1O_2$)	1.2	5.7	11.1-16.3
ΔG^{act}_{add} (HO*)	2.8-5.2	n.a.	7.2-9.6
$\Delta G^{act}_{H\text{-}abs}$ (HO*)	7.5-9.7	6.3-9.7	7.6-11.2

To investigate the interaction of the PPRI with each amino acid, the activation energies for each reaction mechanism between the amino acid and $^1O_2$, $^3CDOM^*$, or $HO^\bullet$ (Table 7) were calculated using DFT at the M06-2X/aug-cc-pVDZ level of theory with the implicit solvation model SMD. Linking this data with PPRI sensitization by 1,4-naphthoquinone reveals the likely culprit for each amino acids' degradation. Regarding 1,4-naphthoquinone, both singlet oxygen and excited triplet state CDOM display relatively low temperature dependence as evidenced by the faster observed rate at higher temperatures.

Singlet oxygen has been shown to exclusively degrade histidine at very fast rates ($5\text{-}6 \times 10^7$ $M^{-1}s^{-1}$)[6, 15-17] by attacking the imidazole ring which is consistent with our DFT activation energy computations where $^1O_2$ addition to histidine is the lowest activation energy barrier (1.2 kcal/mol). In contrast, methionine's degradation is expected to be more vulnerable to $^3CDOM^*$, though $^1O_2$ still is responsible for some degradation (~30%)[6] leading to a combined effect and higher methionine transformation which is consistent with the low activation energy (1.6 kcal/mol) needed for single electron

transfer (SET) by $^{3}CDOM^{*}$ to methionine. Singlet oxygen attacks the sulfide group of methionine (1.3×10^{7} M^{-1} s^{-1}) leading to the production of methionine sulfoxide[5, 6, 14, 52] which was confirmed by this study. Methionine may also undergo degradation via HO•-hydrogen abstraction or HO•-addition (6.50×10^{9} $M^{-1}s^{-1}$)[53], but it is less likely as indicated by the higher activation energy barriers. In this study, 1,4-naphthoquinone is capable of degrading tyrosine further than 2-naphthaldehyde likely due to its ability to sensitize $HO^{\bullet}$ radical, which has been shown to attack aromatic compounds such as tyrosine efficiently[53, 54] at high rates ($k_{HO^{\bullet}}^{Tyr} = 1.3 \times 10^{10} M^{-1}s^{-1}$)[53]. Based on the activation energy computations, $^{1}O_2$ addition and $HO^{\bullet}$ hydrogen abstraction are the two most likely culprits for tyrosine's degradation[53, 55]. Still, the hydroxyl radical bimolecular rate constant with tyrosine is four order of magnitudes higher than the singlet oxygen reaction rate constant with tyrosine ($2\text{-}5 \times 10^{6}$ M^{-1} s^{-1})[56] meaning it is a likely source of tyrosine's degradation.

4 Environmental Implication

Dissolved organic nitrogen in the natural in environment is not refractory and is constantly undergoing transformation. The main sinks for free amino acids and DON as a whole are bacterial uptake, phytoplankton uptake, photochemical degradation, and abiotic adsorption[57-60]. Each of these sinks have varying degrees of contribution to the destruction of DON in the natural environment and have varying levels of research focus done on them. Heterotrophic bacteria are both sinks and sources of free amino acids with many of these bacteria being bottom feeders (i.e., benthic). Phytoplankton also rely on amino acids for basic metabolic function through enzymatic breakdown, pinocytosis (ingest dissolved species), and phagocytosis (engulfment of particulate material). Together, phytoplankton and bacterial uptake of FAAs account for between 4 to 75 nm L^{-1} h^{-1} [58, 61-65]. Comparing this to the SRHA-induced photodegradation of the amino acids, the pseudo-first order rate constants ranged from 0.018 h^{-1} to 0.042 h^{-1}.

To identify the most important pathway for consumption of photoviable amino acids, suppose a surface water has a FAAs concentration of 10 μM; the uptake by phytoplankton and bacteria would consume the FAAs in between 133 and 2500 hours whereas the complete photochemical degradation of the FAAs would occur in between 24 and 55 hours. Clearly, the photochemical degradation of photoviable amino acids is a critical pathway for the disappearance of amino acids in the surface waters and plays a more important role in the FAA bioavailability than uptake by phytoplankton and bacteria. This means that many of these autotrophs and heterotrophs must synthesize these amino acids which are quite energy intensive[16].

The photochemical degradation pathways of DFAAs are a major sink of DON, a vital limiting nutrient, in surface waters. A better understanding of these reaction pathways will elucidate the role of EfOM in nitrogen and sulfur cycling and how it impacts biological activity. Two of the photoviable amino acids, methionine and cysteine, are critical sources of dissolved organic sulfur[5, 66, 67] as well as DON. These two amino acids are consumed by bacteria and phytoplankton and undergo phototransformation to yield sulfate and methanesulfonic acid. Of the entire pool of dissolved organic sulfur in the East Atlantic Ocean, roughly two percent is protein-derived meaning these amino acids are an important portion of the DOS pool[5]. By selecting three structurally-unique free amino acids (tyrosine, histidine, and methionine) and three surrogate structural components of CDOM (1,4-naphthoquinone, 2-naphthaldehyde, and umbelliferone), this project aims to better understand how the DFAAs break down in the presence of structurally diverse DOM constituents.

Still, this study does not wholly emulate the natural environment. Dissolved water constituents such as halogens (Br^- and Cl^-), carbonate species (HCO_3^-, CO_3^{2-}), and other present nutrients (NO_3^{2-}) likely impact the FAAs' degradation. Bromide and chloride ions are present in all natural waters, though most prevalent in the coastal and estuarine waters[47, 68]. In these saltwater conditions, $^3CDOM^*$ is capable of direct oxidation halide oxidation leading to reactive halogen species such as $Cl^\bullet$ and $Br^\bullet$ [69], which have bimolecular rate constants spanning several magnitudes of order with varying substrates leading to difficulty in assessing how these impact the FAA degradation. Additionally, $HO^\bullet$ undergoes reaction preferably with Br^- over Cl^- leading to the formation of $BrOH^{\bullet-}$

which continues to propagate other radical species[47, 69] such as $Br_2^{\bullet-}$ and $ClBr^{\bullet-}$. Due to the wide range of potential oxidation potential of $^3CDOM^*$, it is difficult to speculate which pathway, halide oxidation by $HO^\bullet$ or $^3CDOM^*$, is more dominant.

Carbonate species (HCO_3^-, CO_3^{2-}) have also been shown to impact the degradation of several organic pollutants[70, 71] through the production of the carbonate radical, $CO_3^{\bullet-}$. The carbonate radical is produced primarily through the interaction of carbonate or bicarbonate with the hydroxyl radical or $^3CDOM^*$. The steady-state concentration of $CO_3^{\bullet-}$ is likely two orders of magnitude higher than $[HO^\bullet]_{SS}$ and more selective indicating that it may be more important than the hydroxyl radical for compounds containing more oxidizable moieties such as tyrosine's presence of the aromatic phenol. Nitrate (NO_3^{2-}) ions have been shown to induce photo-oxidation via production of the oxide radical ($^\bullet O^-$) followed by its reaction leading to $HO^\bullet$ [72]. Though with the hydroxyl radical being present in such minute concentrations in freshwater, a pollutant more likely to undergo transformation via singlet oxygen or $^3CDOM^*$.

In this study, these reactions were studied at a constant solution temperature which is critical to the reaction rate and also better simulate the natural surface water environment where these reactions predominantly occur. Going forward, studies must pay close attention to the photoreactor conditions to ensure they closely emulate those in reality. Additionally, an expansion to other surrogate DOM compounds could help further elucidate how each component of dissolved organic matter contributes to the sensitization of photochemically produced reactive intermediates, and, further, identify

which are the most critical portions of dissolved organic matter for degrading organic compounds of interest.

5 References

1. Pehlivanoglu-Mantas, E.; Sedlak, D. L., Measurement of dissolved organic nitrogen forms in wastewater effluents: Concentrations, size distribution and NDMA formation potential. *Water Research* **2008,** *42*, (14), 3890-3898.

2. Qin, C.; Liu, H.; Liu, L.; Smith, S.; Sedlak, D. L.; Gu, A. Z., Bioavailability and characterization of dissolved organic nitrogen and dissolved organic phosphorus in wastewater effluents. *Science of The Total Environment* **2015,** *511*, 47-53.

3. Janssen, E. M. L.; Erickson, P. R.; McNeill, K., Dual roles of dissolved organic matter as sensitizer and quencher in the photooxidation of tryptophan. *Environmental Science and Technology* **2014,** *48*, (9), 4916-4924.

4. Gruber, N.; Galloway, J. N., An Earth-system perspective of the global nitrogen cycle. *Nature* **2008,** *451*, (7176), 293-296.

5. Ksionzek, K. B.; Koch, B. P.; Lechtenfeld, O. J.; McCallister, S. L.; Schmitt-Kopplin, P.; Geuer, J. K.; Geibert, W., Dissolved organic sulfur in the ocean: Biogeochemistry ofa petagram inventory. *Science* **2017,** *356*, (6340), 456-460.

6. Boreen, A. L.; Edhlund, B. L.; Cotner, J. B.; McNeill, K., Indirect photodegradation of dissolved free amino acids: The contribution of singlet oxygen and the differential reactivity of DOM from various sources. *Environmental Science and Technology* **2008,** *42*, (15), 5492-5498.

7. Cottrell, B. A.; Timko, S. A.; Devera, L.; Robinson, A. K.; Gonsior, M.; Vizenor, A. E.; Simpson, A. J.; Cooper, W. J., Photochemistry of excited-state species in natural waters: A role for particulate organic matter. *Water Research* **2013,** *47*, (14), 5189-5199.

8. Wenk, J.; von Gunten, U.; Canonica, S., Effect of Dissolved Organic Matter on the Transformation of Contaminants Induced by Excited Triplet States and the Hydroxyl Radical. *Environmental Science & Technology* **2011,** *45*, (4), 1334-1340.

9. Canonica, S.; Jans, U. R. S.; Stemmler, K.; Hoigne, J., Transformation Kinetics of Phenols in Water: Photosensitization. *Environmental Science & Technology* **1995,** *29*, (7), 1822-1831.

10. Peterson, B. M.; McNally, A. M.; Cory, R. M.; Thoemke, J. D.; Cotner, J. B.; McNeill, K., Spatial and Temporal Distribution of Singlet Oxygen in Lake Superior. *Environmental Science & Technology* **2012,** *46*, (13), 7222-7229.

11. Vaughan, P.; Blough, N., Photochemical Formation of Hydroxyl Radical by Constituents of Natural Waters. *Environmental Science & Technology - ENVIRON SCI TECHNOL* **1998,** *32*.

12. Cooper, W. J.; Zika, R. G., Photochemical Formation of Hydrogen Peroxide in Surface and Ground Waters Exposed to Sunlight. *Science* **1983,** *220*, (4598), 711.

13. Zhang, Y.; Del Vecchio, R.; Blough, N. V., Investigating the Mechanism of Hydrogen Peroxide Photoproduction by Humic Substances. *Environmental Science & Technology* **2012,** *46*, (21), 11836-11843.

14. Remucal, C. K.; McNeill, K., Photosensitized amino acid degradation in the presence of riboflavin and its derivatives. *Environmental Science and Technology* **2011,** *45*, (12), 5230-5237.

15. Chu, C.; Lundeen, R. A.; Remucal, C. K.; Sander, M.; McNeill, K., Enhanced indirect photochemical transformation of histidine and histamine through association with chromophoric dissolved organic matter. *Environmental Science and Technology* **2015,** *49*, (9), 5511-5519.

16. Lundeen, R. A.; Janssen, E. M. L.; Chu, C.; McNeill, K., Environmental photochemistry of amino acids, peptides and proteins. *Chimia* **2014,** *68*, (11), 812-824.

17. Chu, C.; Erickson, P. R.; Lundeen, R. A.; Stamatelatos, D.; Alaimo, P. J.; Latch, D. E.; McNeill, K., Photochemical and Nonphotochemical Transformations of Cysteine with Dissolved Organic Matter. *Environmental Science and Technology* **2016,** *50*, (12), 6363-6373.

18. Appiani, E.; Ossola, R.; Latch, D. E.; Erickson, P. R.; McNeill, K., Aqueous singlet oxygen reaction kinetics of furfuryl alcohol: effect of temperature, pH, and salt content. *Environmental Science: Processes & Impacts* **2017,** *19*, (4), 507-516.

19. Merkel, P. B.; Kearns, D. R., Radiationless Decay of Singlet Molecular Oxygen in Solution. An Experimental and Theoretical Study of Electronic-to-Vibrational Energy Transfer. *Journal of the American Chemical Society* **1972,** *94*, (21), 7244-7253.

20. Snyder, J. W.; Zebger, I.; Gao, Z.; Poulsen, L.; Frederiksen, P. K.; Skovsen, E.; McIlroy, S. P.; Klinger, M.; Andersen, L. K.; Ogilby, P. R., Singlet Oxygen Microscope: From Phase-Separated Polymers to Single Biological Cells. *Accounts of Chemical Research* **2004,** *37*, (11), 894-901.

21. Brahmia, O.; Richard, C., Phototransformation of 1,4-naphthoquinone in aqueous solution. *Photochemical and Photobiological Sciences* **2003,** *2*, (10), 1038-1043.

22. Pflug, N. C.; Schmitt, M.; McNeill, K., Development of N-Cyclopropylanilines to Probe the Oxidative Properties of Triplet-State Photosensitizers. *Environmental Science and Technology* **2019,** *53*, (9), 4813-4822.

23. Yoshihara, T.; Yamaji, M.; Itoh, T.; Shizuka, H.; Shimokage, T.; Tero-Kubota, S., Hydrogen atom transfer and electron transfer reactions in the triplet π,π* state of 1,4-

anthraquinone studied by CIDEP techniques and laser flash photolysis. *Physical Chemistry Chemical Physics* **2000,** *2*, (5), 993-1000.

24. Jaramillo, M.; Joens, J. A.; Shea, K. E. O., Fundamental Studies of the Singlet Oxygen Reactions with the Potent Marine Toxin Domoic Acid. **2020**.

25. Latch, D. E.; McNeill, K., Microheterogeneity of Singlet Oxygen Distributions in Irradiated Humic Acid Solutions. *Science* **2006,** *311*, (5768), 1743-1747.

26. McNeill, K.; Canonica, S., Triplet state dissolved organic matter in aquatic photochemistry: Reaction mechanisms, substrate scope, and photophysical properties. *Environmental Science: Processes and Impacts* **2016,** *18*, (11), 1381-1399.

27. Rosario-Ortiz, F. L.; Canonica, S., Probe compounds to assess the photochemical activity of dissolved organic matter. *Environmental Science and Technology* **2016,** *50*, (23), 12532-12547.

28. Dulin, D.; Mill, T., Development and evaluation of sunlight actinometers. *Environmental Science & Technology* **1982,** *16*, (11), 815-820.

29. Laszakovits, J. R.; Berg, S. M.; Anderson, B. G.; O'Brien, J. E.; Wammer, K. H.; Sharpless, C. M., P-Nitroanisole/pyridine and p-Nitroacetophenone/pyridine actinometers revisited: Quantum yield in comparison to ferrioxalate. *Environmental Science and Technology Letters* **2017,** *4*, (1), 11-14.

30. Tasior, M.; Deperasińska, I.; Morawska, K.; Banasiewicz, M.; Vakuliuk, O.; Kozankiewicz, B.; Gryko, D. T., Vertically π-expanded coumarin – synthesis via the Scholl reaction and photophysical properties. *Physical Chemistry Chemical Physics* **2014,** *16*, (34), 18268-18275.

31. Wolff, T.; Görner, H., Photodimerization of coumarin revisited: Effects of solvent polarity on the triplet reactivity and product pattern. *Physical Chemistry Chemical Physics* **2004,** *6*, (2), 368-376.

32. Simkovitch, R.; Huppert, D., Photoprotolytic Processes of Umbelliferone and Proposed Function in Resistance to Fungal Infection. *The Journal of Physical Chemistry B* **2015,** *119*, (46), 14683-14696.

33. Krauter, C. M.; Möhring, J.; Buckup, T.; Pernpointner, M.; Motzkus, M., Ultrafast branching in the excited state of coumarin and umbelliferone. *Physical Chemistry Chemical Physics* **2013,** *15*, (41), 17846-17861.

34. Murdock, D.; Ingle, R. A.; Sazanovich, I. V.; Clark, I. P.; Harabuchi, Y.; Taketsugu, T.; Maeda, S.; Orr-Ewing, A. J.; Ashfold, M. N. R., Contrasting ring-opening propensities in UV-excited α-pyrone and coumarin. *Physical Chemistry Chemical Physics* **2016,** *18*, (4), 2629-2638.

35. Pinto da Silva, L.; Simkovitch, R.; Huppert, D.; Esteves da Silva, J. C. G., Combined experimental and theoretical study of the photochemistry of 4- and 3-hydroxycoumarin. *Journal of Photochemistry and Photobiology A: Chemistry* **2017,** *338*, 23-36.

36. Simkovitch, R.; Pinto da Silva, L.; Esteves da Silva, J. C. G.; Huppert, D., Comparison of the Photoprotolytic Processes of Three 7-Hydroxycoumarins. *The Journal of Physical Chemistry B* **2016,** *120*, (39), 10297-10310.

37. Alegría, A. E.; Ferrer, A.; Santiago, G.; Sepúlveda, E.; Flores, W., Photochemistry of water-soluble quinones. Production of the hydroxyl radical, singlet oxygen and the superoxide ion. *Journal of Photochemistry and Photobiology A: Chemistry* **1999,** *127*, (1-3), 57-65.

38. Helmut, G., Photoreactions of 1,4-Naphthoquinones: Effects of Substituents and Water on the Intermediates and Reactivity. *Photochemistry and Photobiology* **2005,** *81*, (2), 376-383.

39. Lian, L.; Yan, S.; Zhou, H.; Song, W., Overview of the Phototransformation of Wastewater E ffl uents by High-Resolution Mass Spectrometry. **2020**.

40. Zhou, H.; Yan, S.; Ma, J.; Lian, L.; Song, W., Development of Novel Chemical Probes for Examining Triplet Natural Organic Matter under Solar Illumination. *Environmental Science and Technology* **2017,** *51*, (19), 11066-11074.

41. Sharpless, C. M.; Blough, N. V., The importance of charge-transfer interactions in determining chromophoric dissolved organic matter (CDOM) optical and photochemical properties. *Environmental Sciences: Processes and Impacts* **2014,** *16*, (4), 654-671.

42. Haag, W. R.; Hoigne´, J. r.; Gassman, E.; Braun, A. M., Singlet oxygen in surface waters — Part I: Furfuryl alcohol as a trapping agent. *Chemosphere* **1984,** *13*, (5), 631-640.

43. McCabe, A. J.; Arnold, W. A., Reactivity of Triplet Excited States of Dissolved Natural Organic Matter in Stormflow from Mixed-Use Watersheds. *Environmental Science and Technology* **2017,** *51*, (17), 9718-9728.

44. Varanasi, L.; Coscarelli, E.; Khaksari, M.; Mazzoleni, L. R.; Minakata, D., Transformations of dissolved organic matter induced by UV photolysis, Hydroxyl radicals, chlorine radicals, and sulfate radicals in aqueous-phase UV-Based advanced oxidation processes. *Water Research* **2018,** *135*, 22-30.

45. Moor, K. J.; Schmitt, M.; Erickson, P. R.; McNeill, K., Sorbic Acid as a Triplet Probe: Triplet Energy and Reactivity with Triplet-State Dissolved Organic Matter via 1 O 2 Phosphorescence. *Environmental Science & Technology* **2019,** *53*, (14), 8078-8086.

46. Schmitt, M.; Moor, K. J.; Erickson, P. R.; McNeill, K., Sorbic Acid as a Triplet Probe: Reactivity of Oxidizing Triplets in Dissolved Organic Matter by Direct Observation of Aromatic Amine Oxidation. *Environmental Science & Technology* **2019,** *53*, (14), 8087-8096.

47. Zhang, K.; Parker, K. M., Halogen Radical Oxidants in Natural and Engineered Aquatic Systems. *Environmental Science and Technology* **2018,** *52*, (17), 9579-9594.

48. Wilkinson, F.; McGarvey, D. J.; Olea, A. F., Excited triplet state interactions with molecular oxygen: Influence of charge transfer on the bimolecular quenching rate constants and the yields of singlet oxygen (O2*,1Δg) for substituted naphthalenes in various solvents. *Journal of Physical Chemistry* **1994,** *98*, (14), 3762-3769.

49. Canonica, S.; Hellrung, B.; Wirz, J., Oxidation of phenols by triplet aromatic ketones in aqueous solution. *The Journal of Physical Chemistry A* **2000,** *104*, (6), 1226-1232.

50. Barwise, A. J. G.; Gorman, A. A.; Leyland, R. L.; Smith, P. G.; Rodgers, M. A. J., A pulse radiolysis study of the quenching of aromatic carbonyl triplets by norbornadienes and quadricyclenes. The mechanism of interconversion. *Journal of the American Chemical Society* **1978,** *100*, (6), 1814-1820.

51. Herkstroeter, W. G.; Lamola, A. A.; Hammond, G. S., Mechaisms of Photochemical Reactions in Solution. XXVIII.1 Values of Triplet Excitation energies of Selected Sensitizers. *Journal of the American Chemical Society* **1964,** *86*, (21), 4537-4540.

52. Sysak, P. K.; Foote, C. S.; Ching, T. Y., CHEMISTRY OF SINGLET OXYGEN—XXV. PHOTOOXYGENATION OF METHIONINE*. *Photochemistry and Photobiology* **1977,** *26*, (1), 19-27.

53. Masuda, T.; Nakano, S.; Kondo, M., Rate Constants for the Reactions of OH Radicals with the Enzyme Proteins as Determined by the p-Nitrosodimethylaniline Method. *Journal of Radiation Research* **1973,** *14*, (4), 339-345.

54. Minakata, D.; Li, K.; Westerhoff, P.; Crittenden, J., Development of a Group Contribution Method To Predict Aqueous Phase Hydroxyl Radical (HO•) Reaction Rate Constants. *Environmental science & technology* **2009,** *43*, 6220-7.

55. Matheson, I. B. C.; Lee, J., CHEMICAL REACTION RATES OF AMINO ACIDS WITH SINGLET OXYGEN. *Photochemistry and Photobiology* **1979,** *29*, (5), 879-881.

56. Michaeli, A.; Feitelson, J., REACTIVITY OF SINGLET OXYGEN TOWARD AMINO ACIDS AND PEPTIDES. *Photochemistry and Photobiology* **1994,** *59*, (3), 284-289.

57. Veuger, B.; Middelburg, J. J., Incorporation of nitrogen from amino acids and urea by benthic microbes: role of bacteria versus algae and coupled incorporation of carbon. *Aquatic microbial ecology : international journal* **2007,** *48*, (1), 35-46.

58. Berman, T.; Bronk, D. A., Dissolved organic nitrogen: a dynamic participant in aquatic ecosystems. *Aquatic microbial ecology : international journal* **2003,** *31*, 279-305.

59. Bronk, D. A.; See, J. H.; Bradley, P.; Killberg, L., DON as a source of bioavailable nitrogen for phytoplankton. *Biogeosciences* **2007,** *4*, (3), 283-296.

60. Hansell, D. A.; Carlson, C. A., Biogeochemistry of Marine Dissolved Organic Matter. In Academic Press: US, 2002.

61. Jørgensen, N. O. G.; Kroer, N.; Coffin, R. B., Utilization of Dissolved Nitrogen by Heterotrophic Bacterioplankton: Effect of Substrate C/N Ratio. *Applied and environmental microbiology* **1994,** *60*, (11), 4124-4133.

62. Niels, O. G. J.; Niels, K.; Richard, B. C.; Xiao-Hua, Y.; Cindy, L., Dissolved free amino acids, combined amino acids, and DNA as sources of carbon and nitrogen to marine bacteria. *Marine ecology. Progress series (Halstenbek)* **1993,** *98*, (1/2), 135-148.

63. Rosenstock, B.; Simon, M., Use of dissolved combined and free amino acids by planktonic bacteria in Lake Constance. *Limnology and Oceanography* **1993,** *38*, (7), 1521-1531.

64. Simon, M., Bacterioplankton dynamics in a large mesotrophic lake: II. concentrations and turnover of dissolved amino acids. *Archiv für Hydrobiologie - Hauptbände* **1998,** *144*, (1), 1-23.

65. Schweitzer, B.; Simon, M., Growth limitation of planktonic bacteria in a large mesotrophic lake. *Microbial Ecology* **1995,** *30*, (1), 89-104.

66. Hoffmann, E. H.; Tilgner, A.; Schrödner, R.; Bräuer, P.; Wolke, R.; Herrmann, H., An advanced modeling study on the impacts and atmospheric implications of multiphase dimethyl sulfide chemistry. *Proceedings of the National Academy of Sciences* **2016,** *113*, (42), 11776.

67. Ossola, R.; Tolu, J.; Clerc, B.; Erickson, P. R.; Winkel, L. H. E.; McNeill, K., Photochemical Production of Sulfate and Methanesulfonic Acid from Dissolved Organic Sulfur. *Environmental Science & Technology* **2019,** *53*, (22), 13191-13200.

68. Parker, K. M.; Mitch, W. A., Halogen radicals contribute to photooxidation in coastal and estuarine waters. *Proceedings of the National Academy of Sciences* **2016,** *113*, (21), 5868.

69. Parker, K. M.; Mitch, W. A., Halogen radicals contribute to photooxidation in coastal and estuarine waters. *Proc Natl Acad Sci U S A* **2016,** *113*, (21), 5868-73.

70. Canonica, S.; Kohn, T.; Mac, M.; Real, F. J.; Wirz, J.; von Gunten, U., Photosensitizer Method to Determine Rate Constants for the Reaction of Carbonate Radical with Organic Compounds. *Environmental Science & Technology* **2005,** *39*, (23), 9182-9188.

71. Walse, S. S.; Morgan, S. L.; Kong, L.; Ferry, J. L., Role of Dissolved Organic Matter, Nitrate, and Bicarbonate in the Photolysis of Aqueous Fipronil. *Environmental Science & Technology* **2004,** *38*, (14), 3908-3915.

72. Zepp, R. G.; Hoigne, J.; Bader, H., Nitrate-induced photooxidation of trace organic chemicals in water. *Environmental Science & Technology* **1987,** *21*, (5), 443-450.